Discovery of Novel Zeolites for Natural Gas Purification Through Combined Material Screening and Process Optimization

Eric L. First, M. M. Faruque Hasan, and Christodoulos A. Floudas
Dept. of Chemical and Biological Engineering, Princeton University, Princeton, NJ 08544

DOI 10.1002/aic.14441
Published online March 24, 2014 in Wiley Online Library (wileyonlinelibrary.com)

An efficient computational screening approach is proposed to select the most cost-effective materials and adsorption process conditions for CH_4/CO_2 separation. The method identifies eight novel zeolites for removing CO_2 from natural gas, coalbed methane, shale gas, enhanced oil recovery gas, biogas, and landfill gas sources. The separation cost is minimized through hierarchical material screening combined with rigorous process modeling and optimization. Minimum purity and recovery constraints of 97 and 95%, respectively, are introduced to meet natural gas pipeline specifications and minimize losses. The top zeolite, WEI, can recover methane as economically as \$0.15/MMBTU from natural gas with 5% CO_2 to \$1.44/MMBTU from natural gas with 50% CO_2, showing the potential for developing natural gas reservoirs with higher CO_2 content. The necessity of a combined material selection and process optimization approach is demonstrated by the lack of clear correlation between cost and material-centric metrics such as adsorption selectivity.
 AIChE J, 60: 1767–1785, 2014
Keywords: zeolites, adsorption/gas, process synthesis, optimization, computational screening

Introduction

There are vast reserves of natural gas worldwide that are uneconomical to develop due to high CO_2 content, which can be as high as 70% by volume.[1] About 10% of natural gas in the United States contains significant quantities of CO_2 that must be removed prior to pipeline transportation to meet the typical specification on CO_2 of 3%.[2,3] Typical specifications on composition for U.S. pipelines are provided in Table 1. Even for natural gas sources with low to moderate CO_2 content that is separated before pipeline transport, the CO_2 is often vented into the atmosphere, which contributes to global climate change. In fact, natural gas production is the second-largest source of CO_2 emissions in the United States (after fossil fuel consumption).[5] Even more of an environmental concern is methane, which is the most potent greenhouse gas (GHG) with about 21 times the GHG warming potential than CO_2. It is, therefore, important to minimize methane losses during natural gas purification for both economic and environmental reasons.

Major methane sources in the United States that may require CO_2 separation are illustrated in Figure 1. Shale gas sources typically contain 0–10% CO_2, but the CO_2 content can increase during the life of a well to up to 30%.[6] Coalbed methane is a type of natural gas found in unmineable coal areas, which is typically extracted through the addition of CO_2 that is selectively adsorbed in the coal bed. As a result, coalbed methane typically contains 30–50% CO_2.[7] The gases resulting from enhanced oil recovery may contain 20–80% CO_2 in addition to CH_4.[8] Biogas is the result of anaerobic decomposition of organic waste, such as animal products (e.g., manure), agricultural residues, municipal solid waste, and municipal wastewater. It is primarily a CH_4/CO_2 mixture with CO_2 levels typically 25–45%.[9] Landfill gas is a particularly important type of biogas that contains approximately 40–60% CH_4 with the balance mainly CO_2.[8,10] Collecting and separating these gases would not only reduce GHG emissions but also provide additional sources of energy.

Pressure swing adsorption (PSA) has been previously proposed as a technology suitable for CH_4/CO_2 separation[3] typically using a zeolite (e.g., 13X,[10,14] 4A,[15] or silicalite[16]), metal-organic framework (MOF)[17–21], zeolitic imidazolate framework,[22,23] activated carbon,[24] sepiolite,[25] or polymer[26] as the sorbent. For zeolites and MOFs,[27] for which there exist databases containing thousands of possible candidates, an efficient computational screening procedure is required. Such methods have been developed to identify zeolites[28] and MOFs[29] for membrane-based natural gas purification systems. Kim et al.[30] recently screened zeolites and liquid solvents for methane purification from sources with low to moderate CO_2 content.

In addition to material screening, the PSA process for CH_4/CO_2 separation has also been investigated.[8,31–33] Santos et al.[34] studied the upgrading of biogas (a mixture of CH_4 and CO_2) using a two-column PSA process and evaluated

Additional Supporting Information may be found in the online version of this article.

Eric L. First and M. M. Faruque Hasan contributed equally to this work.

This contribution was identified by Norberto Lemcoff (Rensselaer Polytechnic Institute Hartford) as the Best Presentation in the session "Adsorption Applications for Sustainable Energy" of the 2013 AIChE Annual Meeting in San Francisco, CA.

Correspondence concerning this article should be addressed to C. A. Floudas at floudas@titan.princeton.edu.

Table 1. Typical U.S. Natural Gas Pipeline Specifications[4]

Component	Maximum Concentration
Methane	75 mol % (min)
Ethane	10 mol %
Propane	5 mol %
Butanes	2 mol %
Pentanes and heavier	0.5 mol %
CO_2	3 mol %
N_2 and other inerts	3 mol %
O_2	1 mol %
H_2O	110 mg/m^3
H_2S	7 mg/m^3

the potential of recycle streams. Although high purity (99%) was achieved, low recovery (85%) resulted in significant methane loss to the atmosphere. Cavenati et al.[35–38] utilized both equilibrium and kinetic-based separation and proposed a vacuum swing adsorption (VSA) process to remove CO_2 from a mixture of CH_4, CO_2, and N_2. Although fuel-grade CH_4 purity was attained, the highest CH_4 recovery was about 90%. The same group[37] also evaluated the use of a VSA process for upgrading methane from landfill gas and studied the effect of layered PSA to separate CH_4.[38,39] Spoorthi et al.[40] examined the feasibility of PSA process intensification to reduce plant size and energy consumption for the separation of CH_4 from synthetic landfill gas and lean natural gas.

Despite the plethora of studies concerning material selection and process development for methane recovery, none to date has considered material selection and process optimization in tandem. We have recently shown for CO_2/N_2 separation[41] that proper material selection in tandem with process optimization is critical to achieve the most cost-effective adsorption process. Simultaneous material selection and process optimization is equally important for CH_4/CO_2 separation. In this work, we propose a novel and efficient computational framework to identify the optimal zeolites and process conditions for CH_4/CO_2 separation for a variety of feed pressures and compositions. Using this framework, we identify cost-effective zeolites that have not been previously considered for this application. We also show that material-centric metrics alone are insufficient to predict the lowest-cost separations.

Methods

We have developed a novel hierarchical computational screening approach that combines discovery of zeolitic materials with optimization of an adsorption process. The overall approach is described in Figure 2. This is a new multiscale framework in which the pore systems of candidate zeolites are characterized geometrically, and several material screening metrics are calculated, including shape selectivity, size selectivity, and pore selectivity. Then, adsorption selectivity for suitable zeolites is evaluated. Zeolites that remain after filtering are subject to detailed mathematical modeling and optimization of the PSA process to calculate the minimal cost, which represents the final ranking criterion.

Hierarchical material screening

We propose a novel screening approach to select a short list of candidate materials for CH_4/CO_2 separation from large databases of possible sorbents. The hierarchical approach is designed to efficiently select materials based on performance on one or more metrics. The novel features of the hierarchical screening approach include:

1. geometric-level pore topology characterization via ZEOMICS[42] and MOFomics[43];
2. several unique metrics including shape, size, and pore selectivities;
3. atomistic-level molecular simulations on only a subset of the original databases; and
4. adsorption selectivity as a screening stage rather than the final ranking criterion.

Candidate sorbents are first evaluated using the three-dimensional (3D) pore characterization tools ZEOMICS[42] and MOFomics.[43] These methods apply graph, geometry, and optimization algorithms to the crystallographic data of a microporous material to generate a detailed description of the portals, channels, and cages that comprise the accessible pores. Quantitative properties such as pore size distribution, accessible volume, and accessible surface area are also computed. Pore characterizations for all zeolites studied are freely available online.[44]

Based on the pore characterizations, a number of metrics are calculated to select zeolites with potential for the CH_4/CO_2 separation. The first of these metrics is shape selectivity,[45–48] which describes the degree to which a zeolite can separate two molecules based on a difference in the energetic cost of transport through the pores. The energetic cost for a molecule to traverse a pathway through a 3D porous network is calculated by taking the maximum portal activation energy, E_a, along the pathway, as this represents the pathway's bottleneck.[48] As molecules tend to prefer passing through portals with low activation energies, we identify the

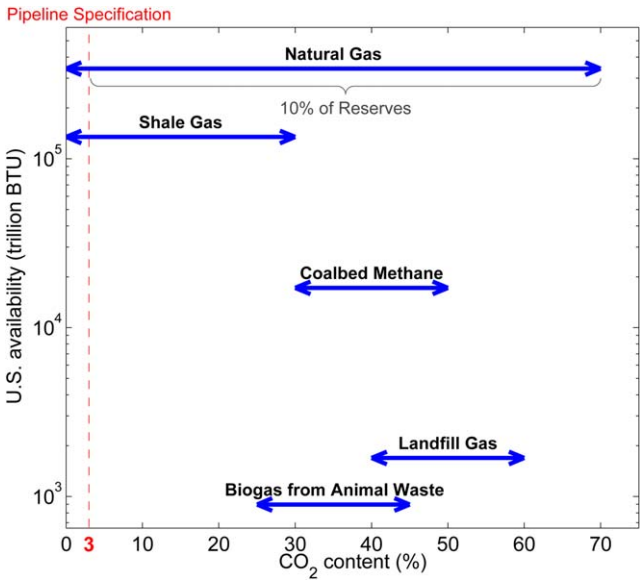

Figure 1. Energy generating potential and range of CO_2 levels of methane sources in the United States.[1,6–13]

Natural gas requiring CO_2 separation to meet pipeline specifications (i.e., CO_2 content >3%) comprises 10% of the total natural gas reserves. Landfill gas and biogas from animal waste are continuous sources, and a period of 20 years is assumed. [Color figure can be viewed in the online issue, which is available at wileyonlinelibrary.com.]

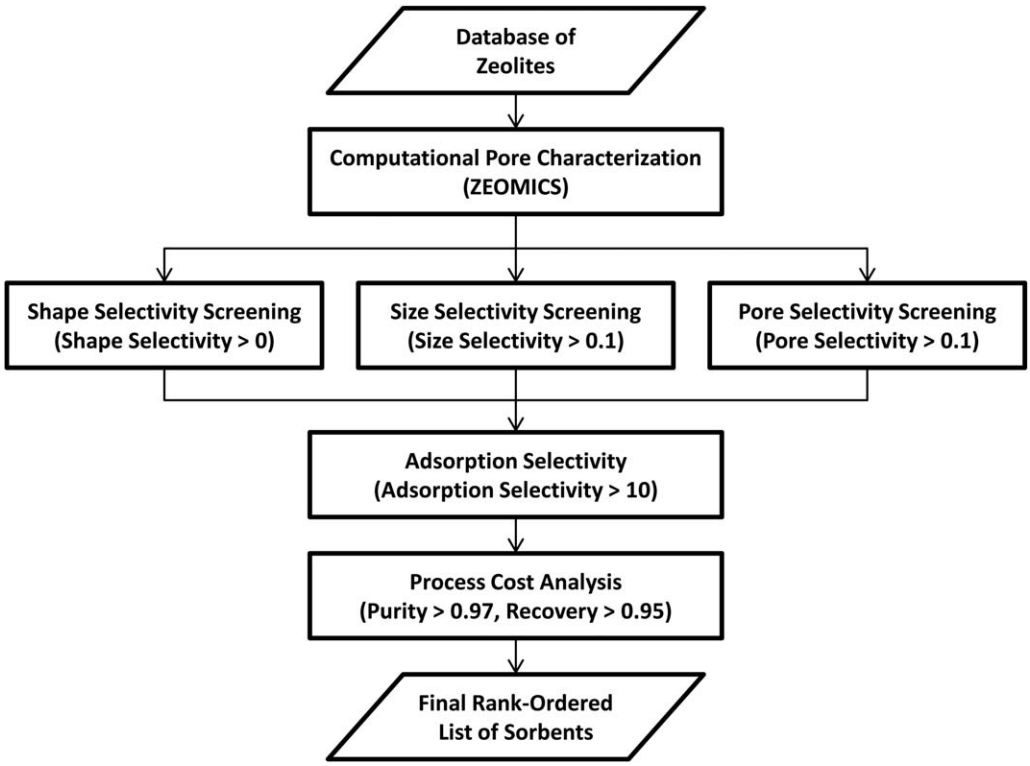

Figure 2. Flowchart of combined material selection and process optimization method for natural gas purification.

minimum energy pathway through the zeolite. The energy of this most dominant pathway, E_p, is found by

$$E_p = \min_{\text{pathways } i} \max_{\substack{\text{portals } j \\ \text{along pathway } i}} E_a^j \tag{1}$$

This bilevel optimization can be represented and solved efficiently as a mixed-integer linear optimization model as described by First et al.[48] Shape selectivity, S_{shape}, between CH_4 and CO_2 in a zeolite is then calculated as

$$S_{shape} = \left| \exp\left(-\frac{E_p^{CH_4}}{RT}\right) - \exp\left(-\frac{E_p^{CO_2}}{RT}\right) \right| \tag{2}$$

where R is the gas constant and $T = 298$ K is the temperature. Note that $S_{shape} \in [0, 1]$, where a value close to 0 indicates low selectivity (i.e., both molecules have similar energetic costs), and a value close to 1 indicates high selectivity (i.e., one molecule can traverse almost freely, whereas the other is severely hindered).

The next metric is size selectivity,[41,42] which is the relative difference in accessible pore volume between CH_4 and CO_2. Accessible pore volume, V_p, is calculated using hard spheres (of diameters 0.396 nm for CH_4 and 0.340 nm for CO_2), and size selectivity, S_{size}, is computed by

$$S_{size} = \frac{|V_p^{CH_4} - V_p^{CO_2}|}{\max\left\{V_p^{CH_4}, V_p^{CO_2}\right\}} \tag{3}$$

Note that $S_{size} \in [0, 1]$, where a value close to 0 indicates low selectivity (i.e., both molecules are accessible to similar pores), and a value close to 1 indicates high selectivity (i.e., one molecule is excluded from most of the pores that the other accesses).

A new metric that we present here for the first time is pore selectivity, which combines the shape-based energetic calculations of shape selectivity with pore accessibility calculations of size selectivity. The reduced equilibrium concentration, C/C_0, of a molecule passing through a zeolite portal is equal to the Boltzmann factor of the portal activation energy, E_a, defined as[45]

$$\frac{C}{C_0} = \exp\left(-\frac{E_a}{RT}\right) \tag{4}$$

The volume accessible to various fractions of guest molecules can be calculated by deeming portals impassible that violate a chosen cutoff value for C/C_0. As the unit cell of a zeolite has a finite number of portals, let P be the set of C/C_0 cutoff values in descending order for which the accessible volume V_i changes. Note that as cutoff C/C_0 decreases, the accessible volume V_i increases as more portals will exceed the threshold, opening up additional pores. Then, the accessible volume, V_a, for a molecule is defined as a weighted summation of incremental volumes by

$$V_a = \sum_{i=1}^{|P|} \left(\frac{C}{C_0}\right)_i (V_i - V_{i-1}) \tag{5}$$

where $V_0 = 0$. Finally, pore selectivity, S_{pore}, is calculated in a similar fashion to size selectivity using the energetically influenced volumes by

$$S_{pore} = \frac{|V_a^{CH_4} - V_a^{CO_2}|}{\max\left\{V_a^{CH_4}, V_a^{CO_2}\right\}} \tag{6}$$

Note that $S_{pore} \in [0, 1]$ with a similar interpretation to S_{size}. Pore selectivity has the advantage of being based on actual molecule shapes, rather than an approximation based on hard spheres, which is particularly important for CH_4, which has a noncircular footprint.

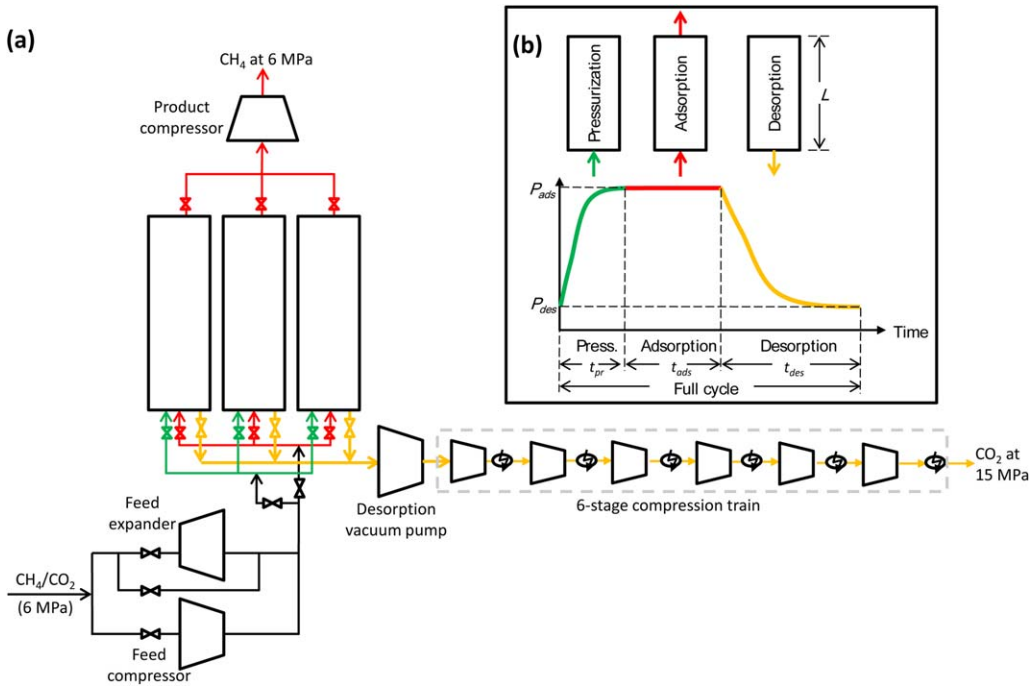

Figure 3. PSA process for methane recovery from natural gas, coalbed methane, shale gas, enhanced oil recovery gas, biogas, or landfill gas sources.

The process flow diagram (a) includes options for feed compression or expansion and one or multiple adsorption columns. Desorption vacuum pump, CH_4 product compression, and CO_2 compression are considered. The adsorption cycle consists of three steps, pressurization, adsorption, and countercurrent desorption, with a representative pressure profile and step durations indicated in the inset (b). A complete description of the adsorption process is found in the main text. [Color figure can be viewed in the online issue, which is available at wileyonlinelibrary.com.]

Each of the metrics of shape-, size-, and pore-selectivity is readily computable from the automated 3D zeolite pore characterizations. We have devised a screening criterion to filter the database of candidate zeolites down to a smaller number suitable for more detailed atomistic-level calculations. Zeolites are selected that meet at least one of (1) $S_{\text{shape}} > 0$, (2) $S_{\text{size}} > 0.1$, or (3) $S_{\text{pore}} > 0.1$. For these filtered structures, grand canonical Monte Carlo (GCMC) simulations are used to calculate adsorption selectivity, S_{ads}, defined as the ratio of Henry constants, H_i, by

$$S_{\text{ads}} = \frac{H_{\text{CO}_2}}{H_{\text{CH}_4}} \tag{7}$$

The details of the GCMC simulations are provided in Appendix A. Note that the adsorption isotherm needs to be evaluated at just two low-pressure points at one temperature (298 K) to estimate the Henry constant from the adsorption isotherm slope. We select zeolites with $S_{\text{ads}} > 10$ and compute full adsorption isotherms over a range of five temperatures (298–398 K) to fit to a dual-site Langmuir model (see Eqs. A1–A3 in Appendix A for details). The isotherm parameters for each zeolite are used for the subsequent modeling and optimization of the adsorption process.

Process modeling and optimization of PSA

We consider a simple PSA process for the separation of CH_4 and the capture and compression of CO_2 for utilization and/or sequestration from a CH_4/CO_2 mixture. The process is designed to address a range of feed conditions that represent a variety of CO_2-rich natural gas, coalbed methane, shale gas, enhanced oil recovery gas, biogas, and landfill gas sources in the United States. It allows for either expansion or compression of the feed and compression of products CH_4 and CO_2, which are crucial for determining the optimal adsorption pressure and meeting pipeline specifications. The novel features of the proposed process include:

1. either compression or expansion of the feed to achieve the optimal adsorption pressure;
2. methane product compression to pipeline pressure of 6 MPa;
3. CO_2 capture coupled with compression for sequestration at 15 MPa;
4. independently operating multiple and identical adsorption columns; and
5. power integration between the feed expander and the product compressor to minimize energy consumption.

The overall PSA process is shown in Figure 3a. First, the feed, which is a mixture of CH_4 and CO_2, is either compressed or expanded to achieve the desired adsorption pressure, P_{ads}. This differs from the CO_2 capture process,[41] which does not have the option for feed expansion. Expansion can occur with either a pressure relief valve or an expansion turbine, which produces electricity that can be used for feed or product compression. The tradeoff between investment cost and electric utility determines whether an expansion turbine is economical depending on the feed flow rate and adsorption pressure. Next, one or multiple identical zeolite-packed adsorption columns are used for adsorption. Because CO_2 is selectively adsorbed over CH_4 in many zeolites, most of the CH_4 fed into a column passes through without being adsorbed. The clean CH_4 is then compressed to 6 MPa to meet the specification for pipeline transportation. The product compressor is run by electricity that is

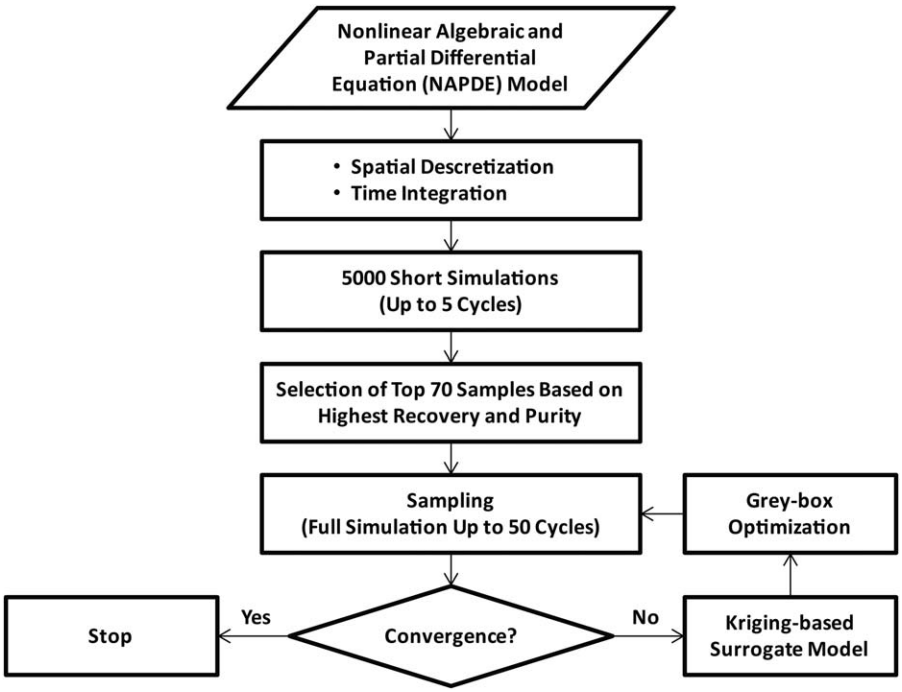

Figure 4. Flowchart for Kriging-based grey-box constrained optimization.

either taken from the grid or produced by the feed expander, if it is selected. A desorption vacuum pump at the feed-end of the column is used to evacuate the adsorbed CO_2 at the lowest vacuum level, P_{des}. The CO_2 is compressed to 15 MPa for sequestration using a six-stage compression train with intercoolers and a pressure ratio of 2.3 at each stage.

PSA is a cyclic process in which CO_2 alternately adsorbs and desorbs to the zeolite sorbent within the adsorption columns. We utilize a simple three-step PSA cycle, illustrated in Figure 3b, which includes (1) column pressurization, (2) CO_2 adsorption and CH_4 product recovery, and (3) countercurrent desorption of CO_2. During pressurization, feed gas enters each column from one end (green lines in Figure 3a) while the other end is closed. During adsorption, both ends of the column are open (red lines), and CO_2 adsorbs at P_{ads} while CH_4 is collected as product. During desorption, CO_2 is evacuated (yellow lines) from the feed-end of the column at the lowest pressure (P_{des}) in the cycle. Being a cyclic process, the process undergoes a transient state for a number of cycles before reaching cyclic steady state at which point performance is measured.

The PSA process is modeled using a detailed nonlinear algebraic and partial differential equation (NAPDE) system, which is presented in Appendix B. It consists of coupled nonlinear partial differential equations that describe the mass and energy balances and fluid flow through porous media. The model considers a multicomponent adsorption system with temperature, pressure, and velocity effects and heat-transfer resistance across the column wall.[49] For each candidate zeolite, the adsorption process is optimized to select the best assignment of the decision variables, which include the column length (L), adsorption (P_{ads}) and desorption (P_{des}) pressures, and adsorption (t_{ads}) and desorption (t_{des}) step durations. The pressurization time, column diameter, and number of columns are also determined for each zeolite.

To address the challenge of optimizing a large and complex NAPDE model, we have developed an efficient Kriging-based grey-box constrained optimization approach,[41,50] which can optimize the NAPDE model in reasonable time. The Kriging-based surrogate model of the original NAPDE model is described in detail in Appendix C. A robust and automated grey-box constrained optimization routine uses both the NAPDE model and Kriging-based surrogate model to optimize the PSA process for each candidate zeolite and generate a rank-ordered list of cost-effective sorbents. Our approach consists of generating input–output data by solving the NAPDE model at several sample conditions, using these data to develop a Kriging-based surrogate model, and optimizing the surrogate model to determine additional sample conditions. This process is repeated until convergence to an optimal solution.

Figure 4 outlines a more detailed description of our grey-box constrained optimization algorithm. To evaluate the NAPDE model at fixed conditions, we discretize over both space and time. We perform 5000 short simulations with initial sample conditions selected using a Latin Hypercube design to scan through the ranges of all variables. The process performance at each of these conditions is estimated using short simulations consisting of only five cycles. The top 70 samples based on purity and recovery are selected for full simulations in which the discretized NAPDE model is solved to near cyclic steady state using up to 50 cycles. The resulting purity, recovery, and cost data for these samples are used to construct the initial Kriging model via parameter estimation (see model M1 in Appendix C). This surrogate model is optimized to identify the next sample point, which is simulated to near cyclic steady state with up to 50 cycles. If the purity, recovery, and cost results from the full simulation are within 0.1% of the surrogate model estimation, the algorithm reaches convergence. Otherwise an updated

Table 2. Decision Variables used in the Adsorption Process Model and their Corresponding Operating Ranges, Before and After Bound Refinement, and the Subdivisions Corresponding to the Three Branching Variables

Variable	Original Bounds	Refined Bounds	Subdivisions
L (m)	[1, 4]	[1, 1]	–
P_{ads} (kPa)	[100, 6000]	[100, 500]	[100, 300], [300, 500]
P_{des} (kPa)	[1, 100]	[1, 10]	–
t_{ads} (s)	[20, 100]	[40, 100]	[40, 70], [70, 100]
t_{des} (s)	[20, 150]	[20, 150]	[20, 80], [80, 150]

Kriging model is constructed to identify the next sample point. The process conditions corresponding to the best cost after convergence or 250 iterations, whichever occurs first, is used as the solution to the NAPDE model optimization.

For each zeolite, the grey-box constrained optimization algorithm is applied using broad initial variable bounds, which are listed in Table 2. The bounds on pressures take into account industrial vacuum capabilities and the bounds on step durations ensure that stability can be achieved at each pressure level. Based on the ranges of optimal conditions attained for the set of candidate zeolites, the decision variable bounds are refined to tighten the sets of values to consider and are listed in Table 2. To aid in the search for globally optimal solutions, the search domain is subdivided by splitting the ranges of three decision variables, P_{ads}, t_{ads}, and t_{des}, as indicated in Table 2, to form eight subdomains. The proposed grey-box constrained optimization algorithm is applied for each feasible zeolite and each subdomain, and the best overall result is used.

Results and Discussion

From the database of 199 zeolites available in ZEOMICS,[42,44] we identify 26 that are shape selective, 50 that are size selective, and 43 that are pore selective, as listed in Table 3. There are 86 distinct zeolites in the union, with several zeolites scoring well on multiple metrics and three zeolites (CAS, CGF, and NSI) appearing in all three lists. From the zeolites with shape, size, and/or pore selectivity, we evaluate adsorption selectively and find 22 that are adsorption-selective and suitable for process optimization (see Table 4). Refer to the Supporting Information for a detailed description of each of these zeolites, including properties, adsorption isotherms, and results. Note that six zeolites are excluded from analysis because of difficulties with the molecular simulations—LIT due to a charge imbalance from protruding oxygen atoms and BCT, CHI, MTN, MVY, and VSV due to no CH_4 molecules being adsorbed.

We consider feed conditions typical of natural gas, coalbed methane, shale gas, enhanced oil recovery gas, biogas, and landfill gas sources. The representative feed CO_2 compositions used in our computational studies include 5, 10, 20, 30, 40, and 50%. We use a feed pressure of 6 MPa, which is typical of natural gas sources and subsequently explore the effect of lower feed pressures. The feed flow rate is 0.1 kmol/s, which is typical for a single-train adsorption process. A minimum purity of 97% on the product methane is imposed to meet pipeline specifications, and a minimum recovery of 95% is imposed to limit product losses and GHG emissions.

For each feed condition, the NAPDE model describing the PSA process is optimized for each candidate zeolite to obtain the minimum process cost and corresponding performance in regard to purity and recovery. The cost-effective zeolites for each feed condition are provided in Table 5, and detailed cost breakdowns can be found in Supporting Information Tables 1–6. Of the 22 adsorption-selective zeolites, eight are feasible for all feed conditions (ABW, AEN, AHT, APC, BIK, JBW, MON, and WEI), and two additional zeolites are feasible for only 5% CO_2 in the feed (LTJ and NSI). These 10 zeolites are listed in Table 6 with their corresponding minimum costs for each feed condition. Many of these feasible zeolites have similar process costs at each feed condition, though zeolite WEI is always at least tied for the most cost-effective zeolite for all feed CO_2 compositions. The zeolites AHT and AEN are also consistently in the top five (see illustration of the top zeolites in Figure 5).

Table 3. Shape-, Size-, and Pore-Selective Zeolites for CH_4/CO_2 Separation

Shape Selectivity		Size Selectivity		Pore Selectivity	
Zeolite	S_{shape}	Zeolite	S_{size}	Zeolite	S_{pore}
DOH	0.83	AEN	1.00	MTN	1.00
GIU	0.78	AFN	1.00	LIT	1.00
SOD	0.75	APC	1.00	AFG	1.00
FRA	0.74	APD	1.00	LOS	1.00
FAR	0.60	BIK	1.00	RUT	1.00
LOS	0.60	BRE	1.00	SGT	1.00
MVY	0.53	CAS	1.00	ANA	0.99
TOL	0.45	CDO	1.00	MSO	0.99
ANA	0.44	CGF	1.00	FAR	0.98
MAR	0.42	CHI	1.00	SOD	0.98
AHT	0.40	ESV	1.00	MEP	0.98
CGF	0.31	GIS	1.00	MAR	0.97
CAS	0.26	GOO	1.00	NON	0.97
NON	0.25	JBW	1.00	GIU	0.96
AFG	0.09	JRY	1.00	DOH	0.95
MSO	0.08	JST	1.00	AST	0.95
SGT	0.07	LOV	1.00	TOL	0.94
BRE	0.06	LTJ	1.00	LIO	0.85
NSI	0.06	MON	1.00	LTN	0.84
AST	0.02	NSI	1.00	FRA	0.83
MTN	0.02	PON	1.00	MVY	0.80
LTN	0.01	RSN	1.00	BCT	0.64
LIO	0.01	RWR	1.00	AHT	0.44
MEP	0.01	SAT	1.00	CGF	0.39
LIT	0.01	SBN	1.00	ABW	0.30
RUT	0.00	VSV	1.00	CAS	0.29
		WEI	1.00	TON	0.29
		YUG	1.00	JBW	0.26
		LTF	0.64	APC	0.20
		IWW	0.62	SFE	0.19
		MAZ	0.61	NSI	0.18
		ZON	0.58	VFI	0.17
		SIV	0.54	MTW	0.17
		NPT	0.53	SFN	0.15
		MER	0.51	ATS	0.13
		GME	0.47	BIK	0.13
		MOR	0.45	LAU	0.12
		DAC	0.45	SSF	0.12
		AFX	0.41	NAT	0.12
		SOF	0.40	AFO	0.11
		SZR	0.38	ATV	0.11
		MEI	0.36	LTL	0.10
		PAU	0.33	MAZ	0.10
		AFT	0.28		
		DFT	0.27		
		MFS	0.24		
		OBW	0.20		
		EDI	0.17		
		THO	0.13		
		TSC	0.12		

Table 4. Adsorption-Selective Zeolites for CH_4/CO_2 Separation

Zeolite	LCD (nm)	PLD (nm)	Shape Selectivity	Size Selectivity	Pore Selectivity	Adsorption Selectivity
AHT	0.46	0.34	0.40	0	0.44	110583.76
WEI	0.39	0.39	0	1.00	0.04	4916.51
NSI	0.48	0.34	0.06	1.00	0.18	976.49
MON	0.49	0.35	0	1.00	0.05	484.80
ABW	0.41	0.41	0	0	0.30	458.25
BIK	0.48	0.36	0	1.00	0.13	416.51
JBW	0.38	0.38	0	1.00	0.26	365.20
APC	0.49	0.38	0	1.00	0.20	237.36
AEN	0.51	0.37	0	1.00	0	236.76
RWR	0.51	0.38	0	1.00	0	65.59
YUG	0.51	0.37	0	1.00	0	52.07
GIS	0.56	0.39	0	1.00	0	36.76
PON	0.45	0.39	0	1.00	0.03	26.33
SIV	0.60	0.44	0	0.54	0	24.84
LTJ	0.37	0.37	0	1.00	0.02	23.18
GOO	0.51	0.36	0	1.00	0.06	16.30
RSN	0.58	0.34	0	1.00	0.02	14.84
DFT	0.57	0.43	0	0.27	0	14.09
ANA	0.49	0.30	0.44	0	0.99	12.60
LOV	0.58	0.34	0	1.00	0.02	12.26
PAU	1.11	0.47	0	0.33	0.01	11.47
MER	0.73	0.48	0	0.51	0	10.26

For 5% CO_2, all feasible zeolites have similar costs, which range from \$0.15 to \$0.16/MMBTU (1 MMBTU = 293.07 kWh). The costs for feasible zeolites for 10% CO_2 increases to \$0.26–0.28/MMBTU. For 20% CO_2, the range of costs for feasible zeolites is \$0.48–0.52/MMBTU. For 30% CO_2, the costs for feasible zeolites range from \$0.72 to \$0.81/MMBTU. As the feed CO_2 content increases to 40%, the costs also increase to \$1.04–1.20/MMBTU. For a feed consisting of a 50–50 mixture of CO_2 and methane, the costs rise to \$1.44–1.74/MMBTU. Given that the Henry Hub price of pipeline-quality natural gas is \$4.04 (as of May 2013),[51] the low separation costs of removing CO_2 using the identified zeolites and process conditions suggest that it may be cost-effective to exploit natural gas reserves with higher CO_2 contents. The use of these novel zeolites for landfill gas purification is particularly promising given the significantly lower associated production costs. It also makes viable the economic production of methane from biomass.

Table 5. Cost-Effective Zeolites for CH_4/CO_2 Separation from Feeds with 5–50% CO_2

Zeolite	Purity (%)	Recovery (%)	Cost (\$/MMBTU)	Zeolite	Purity (%)	Recovery (%)	Cost (\$/MMBTU)
		5% CO_2				10% CO_2	
ABW	97	98	0.15	WEI	98	98	0.26
AHT	97	99	0.15	ABW	97	98	0.27
APC	97	97	0.15	AEN	97	97	0.27
WEI	97	98	0.15	AHT	98	97	0.27
AEN	97	97	0.16	APC	97	97	0.27
BIK	97	98	0.16	BIK	97	97	0.27
JBW	97	97	0.16	MON	97	96	0.27
LTJ	97	95	0.16	JBW	98	96	0.28
MON	97	97	0.16				
NSI	97	98	0.16				
		20% CO_2				30% CO_2	
AHT	98	97	0.48	WEI	97	97	0.72
WEI	97	97	0.48	AEN	97	97	0.76
AEN	97	97	0.49	APC	97	95	0.76
APC	98	96	0.50	AHT	97	98	0.77
BIK	97	97	0.50	JBW	97	95	0.77
JBW	97	95	0.50	MON	97	97	0.77
MON	97	97	0.50	BIK	98	96	0.80
ABW	97	96	0.52	ABW	98	97	0.81
		40% CO_2				50% CO_2	
WEI	98	98	1.04	WEI	98	97	1.44
AHT	97	97	1.08	AEN	97	96	1.57
AEN	97	95	1.10	MON	98	96	1.59
MON	98	96	1.12	JBW	97	95	1.62
APC	98	96	1.14	AHT	97	98	1.64
BIK	98	96	1.14	BIK	98	97	1.64
JBW	97	95	1.16	APC	97	96	1.65
ABW	98	97	1.20	ABW	98	97	1.74

The listed purity, recovery, and costs are obtained at the optimal process conditions.

Table 6. Cost ($/MMBTU) for Feasible Zeolites at Various Feed Compositions

	Feed CO_2 Content					
Zeolite	5%	10%	20%	30%	40%	50%
ABW	0.15	0.27	0.52	0.81	1.20	1.74
AEN	0.16	0.27	0.49	0.76	1.10	1.57
AHT	0.15	0.27	0.48	0.77	1.08	1.64
APC	0.15	0.27	0.50	0.76	1.14	1.65
BIK	0.16	0.27	0.50	0.80	1.14	1.64
JBW	0.16	0.28	0.50	0.77	1.16	1.62
LTJ	0.16	–	–	–	–	–
MON	0.16	0.27	0.50	0.77	1.12	1.59
NSI	0.16	–	–	–	–	–
WEI	0.15	0.26	0.48	0.72	1.04	1.44

The process costs of the eight zeolites feasible for all feed conditions are plotted in Figure 6 as a function of CO_2 level in the feed. Cost increases somewhat linearly with CO_2 level until about 20%, after which it increases at an increasing rate. Although the feasible zeolites have very similar costs at lower CO_2 levels, the spread in costs increases at higher feed CO_2 concentrations, indicating that the choice of zeolite plays a more important role for CO_2-rich methane sources. It is important to note that zeolite choice is important at all CO_2 levels as most of the zeolites are not able to meet the purity and recovery requirements, making their costs irrelevant. Only 8 of the original 199 zeolites are found to satisfy the purity and recovery constraints, highlighting the importance of material selection combined with process design.

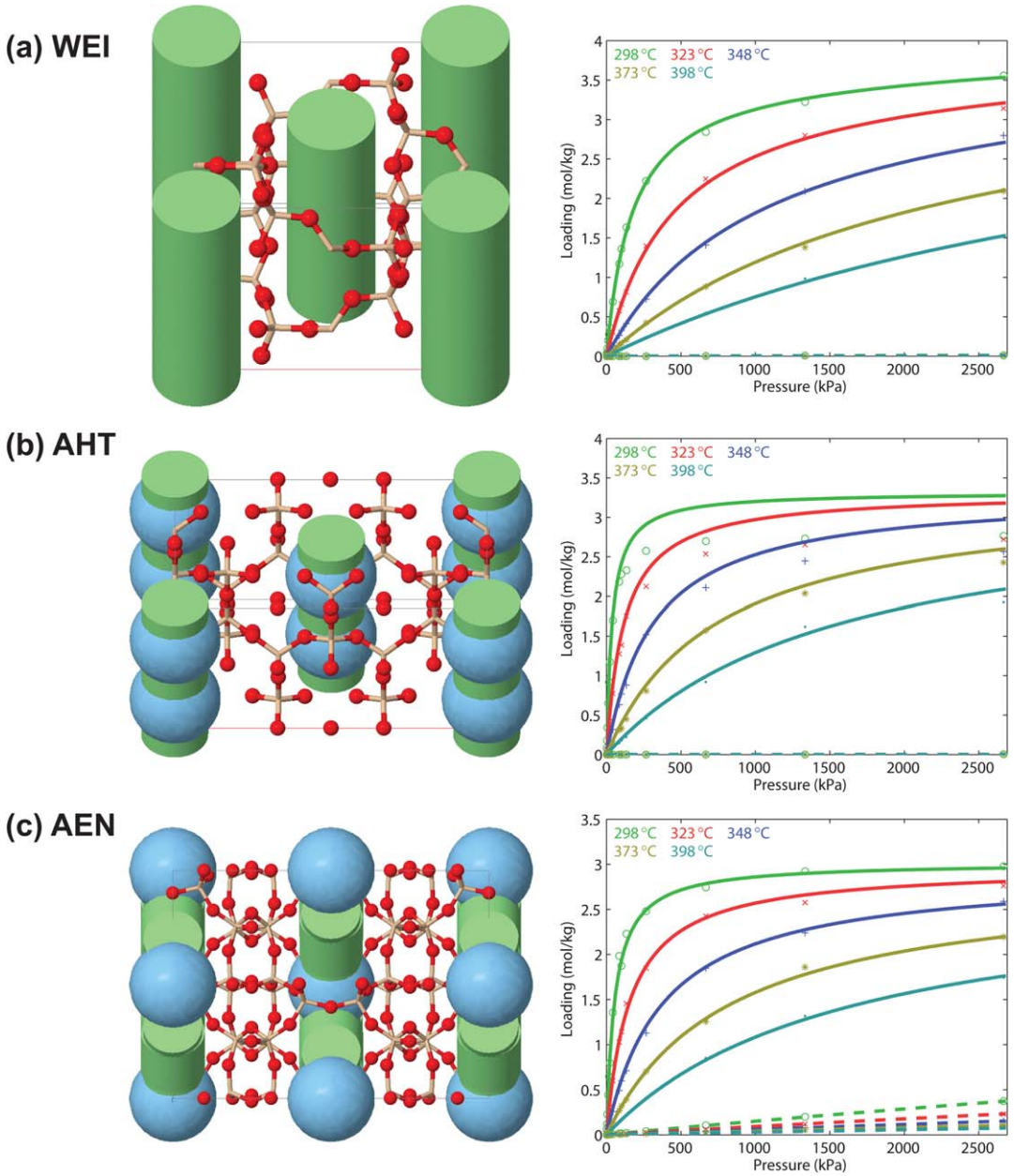

Figure 5. ZEOMICS[42,44] main pore network visualizations and CO_2 and CH_4 adsorption isotherms for zeolites consistently in the top five for each feed condition, (a) WEI, (b) AHT, and (c) AEN.

In the pore display, a unit cell is depicted with channels shown in green and cages in blue. For the adsorption isotherms, GCMC data at five different temperatures are shown with symbols, and the dual-site Langmuir model fitting is shown with solid lines (CO_2) and dashed lines (CH_4). [Color figure can be viewed in the online issue, which is available at wileyonlinelibrary.com.]

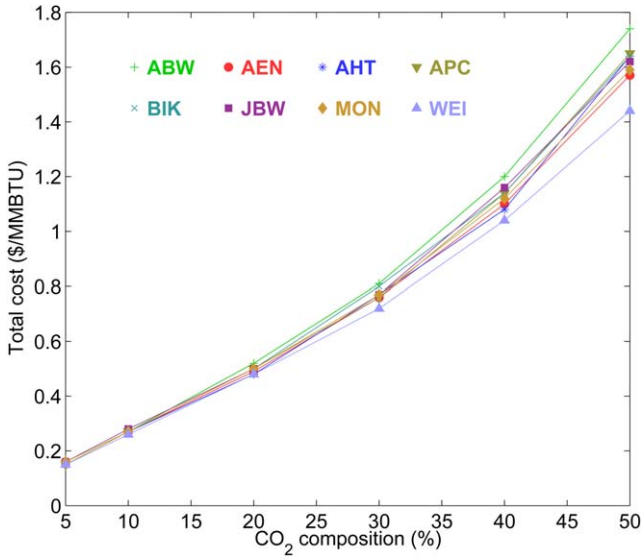

Figure 6. Plot of total cost vs. CO_2 composition for 6 MPa feed.

Zeolites that satisfy purity and recovery constraints for all CO_2 compositions studied (5, 10, 20, 30, 40, and 50%) are shown. Data points are connected with straight line segments to guide the eye. [Color figure can be viewed in the online issue, which is available at wileyonlinelibrary.com.]

Optimal process conditions vary depending on the zeolite and feed composition (see Supporting Information Tables 7–12), and several trends for the eight always-feasible zeolites can be observed (see Figure 7). The average number of columns tends to decrease with increasing CO_2 in the feed, from 2 for 5% CO_2 to 1.1 (typically 1 to be used) to 50% CO_2. This is due to a decrease in the average time for the adsorption step with increasing CO_2, which shortens the total cycle time, along with an increase in desorption time, the longest step in the cycle. Average column diameter increases from 1.05 m for 5% CO_2 in the feed to 2.50 m for 50% CO_2 to accommodate the feed using fewer columns. The column length is always 1 m, the lower bound of the initial domain, indicating that shorter columns are preferred to fully utilize the bed. The average adsorption and desorption pressures decrease with increasing CO_2 levels to mitigate changes in CO_2 partial pressures, which affect adsorption/desorption.

There are additional trends for the eight zeolites feasible for all feed conditions (see Figure 8). With a 5% CO_2 feed, the average investment cost is \$0.12/MMBTU (75% of the total) and the average operating cost is \$0.04/MMBTU (23% of the total). The material cost, which is considered separately from the operating cost, represents about 1–2% of the total cost in all cases, and is based on \$2/kg. Though specialty zeolite synthesis could result in a higher material cost,

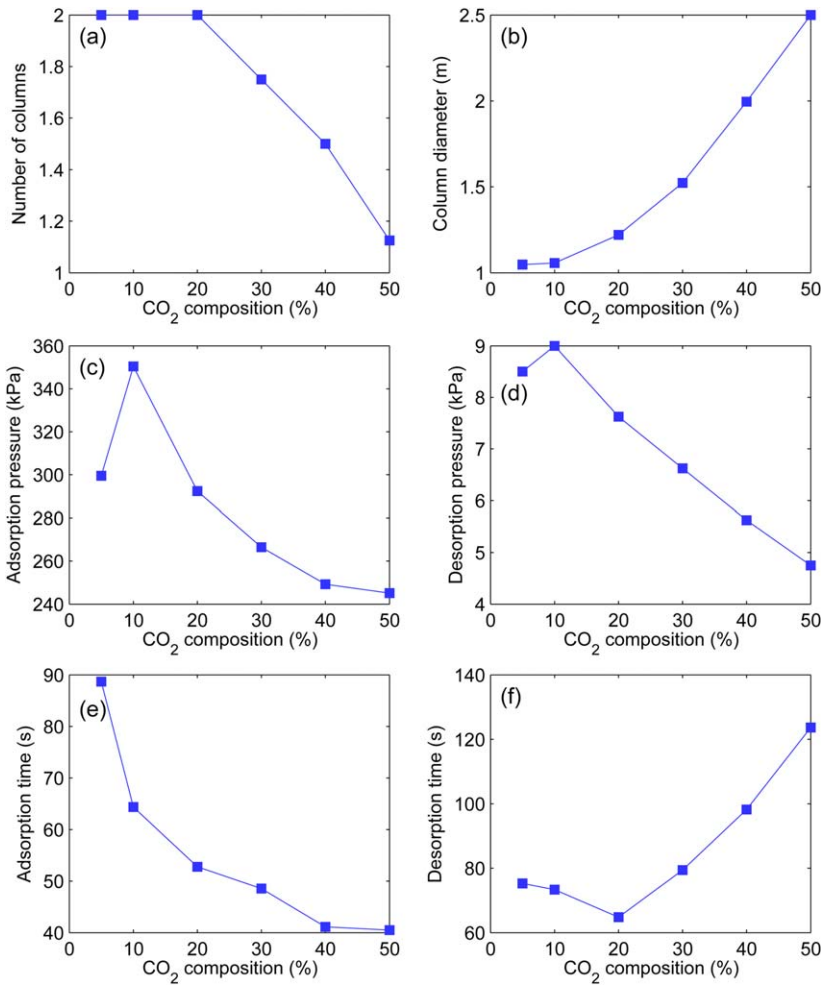

Figure 7. Plots of average process configuration parameters for the eight zeolites feasible for all CO_2 compositions as a function of CO_2 content in the feed.

(a) Number of columns, (b) column diameter, (c) adsorption pressure, (d) desorption pressure, (e) adsorption step time, and (f) desorption step time. [Color figure can be viewed in the online issue, which is available at wileyonlinelibrary.com.]

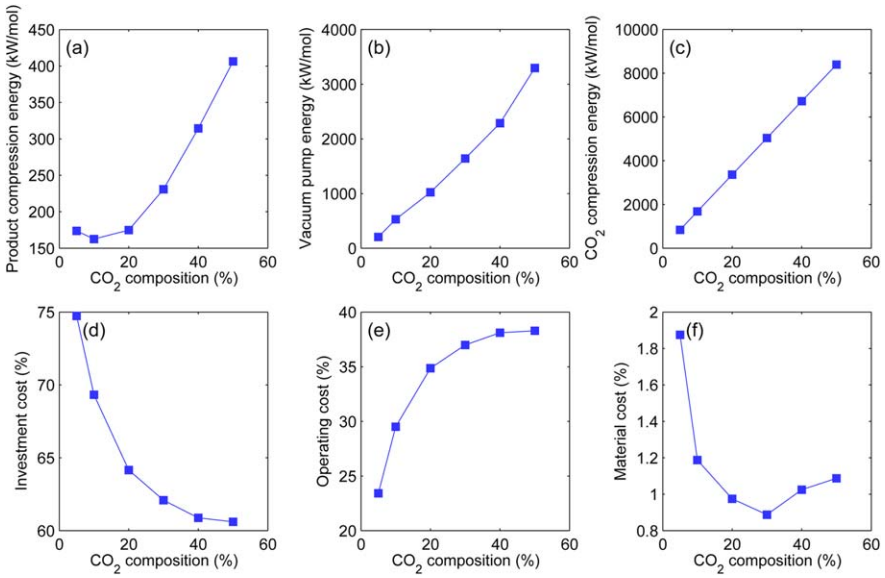

Figure 8. Plots of average energy and cost results for the eight zeolites feasible for all CO_2 compositions as a function of CO_2 content in the feed.

(a) Product compression energy, (b) desorption vacuum pump energy, (c) CO_2 compression energy, (d) investment cost percentage, (e) operating cost percentage, and (f) material cost percentage. [Color figure can be viewed in the online issue, which is available at wileyonlinelibrary.com.]

even a 10-fold increase to \$20/kg corresponds to no more than a 5–19% increase in total cost. Operating cost increases at a faster rate than investment cost as the CO_2 content increases, so that for a feed with 50% CO_2, the average investment cost represents 61% of the total cost and the average operating cost represents 38% of the total (the balance is the material cost). The reason that the operating cost grows to become a larger share of the total for higher CO_2 levels is due to the significant increase in the CO_2 compression energy, as well as the desorption energy.

Some methane sources are available at pressures lower than the 6 MPa typical of natural gas reserves. In general, the feed pressure affects process cost through two means. The first is that a feed pressure greater than the adsorption pressure can be used to recover energy through the use of an expansion turbine. This is only economical for certain combinations of feed pressure, adsorption pressure, and feed flow rate, as illustrated in Figure 9. For our feed flow rate of 0.1 kmol/s, an expansion turbine is never selected regardless of the feed and adsorption pressures. The second is that a feed pressure lower than the adsorption pressure requires the use of a feed compressor, which requires energy input. In our case studies, the optimal adsorption pressure never exceeds 500 kPa, so the cost results will remain the same for any feed pressure of at least 500 kPa.

Previously we found several cost-effective zeolites for the separation of CO_2/N_2 (see Table 6 of Hasan et al.[41]). Comparing the top 10 zeolites for this application with the zeolites identified for the CH_4/CO_2 separation reveals just three in common (ABW, AHT, and WEI). It is reasonable to expect similarities in the results because CO_2 is selectively adsorbed in both systems. The differences arise from the generally higher adsorption of CH_4 than that of N_2. Additionally, the more stringent purity and recovery constraints for methane purification reduce the number of feasible zeolites (26 feasible zeolites identified for CO_2/N_2 compared to 10 in this study). The feed CO_2 composition (14% for the CO_2/N_2 study) and pressure (100 kPa for CO_2/N_2) also play a role in determining the driving force for adsorption.

All the materials considered are silica zeolites from the International Zeolite Association.[52] Of the 10 feasible zeolites, only NSI has been synthesized in a pure silica form,[53] which makes it a good candidate for near term study for 5% CO_2 feeds (note that NSI is not feasible for higher than 5% CO_2 composition). Three zeolites, BIK, MON, and WEI, are naturally occuring, with synthetic analogs available for all

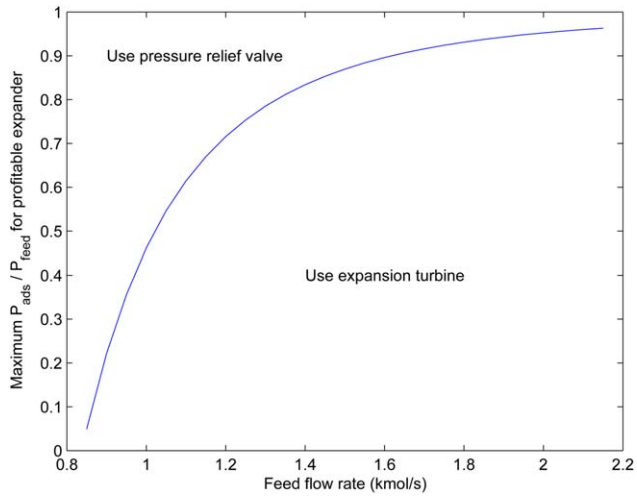

Figure 9. Plot illustrating the tradeoff between investing in an expansion turbine and its electric utility output.

The choice to use an expansion turbine vs. a pressure relief valve depends on the feed flow rate and the adsorption to feed pressure ratio. Note that the boundary curve intersects the horizontal axis at a feed flow rate of about 0.84 kmol/s, indicating that an expansion turbine is not economical for smaller flow rates regardless of the adsorption pressure. This analysis assumes an efficiency of 75%, a temperature of 298 K, and current economic data for the expansion turbine investment cost (annualized over 20 years) and the price of electricity. [Color figure can be viewed in the online issue, which is available at wileyonlinelibrary.com.]

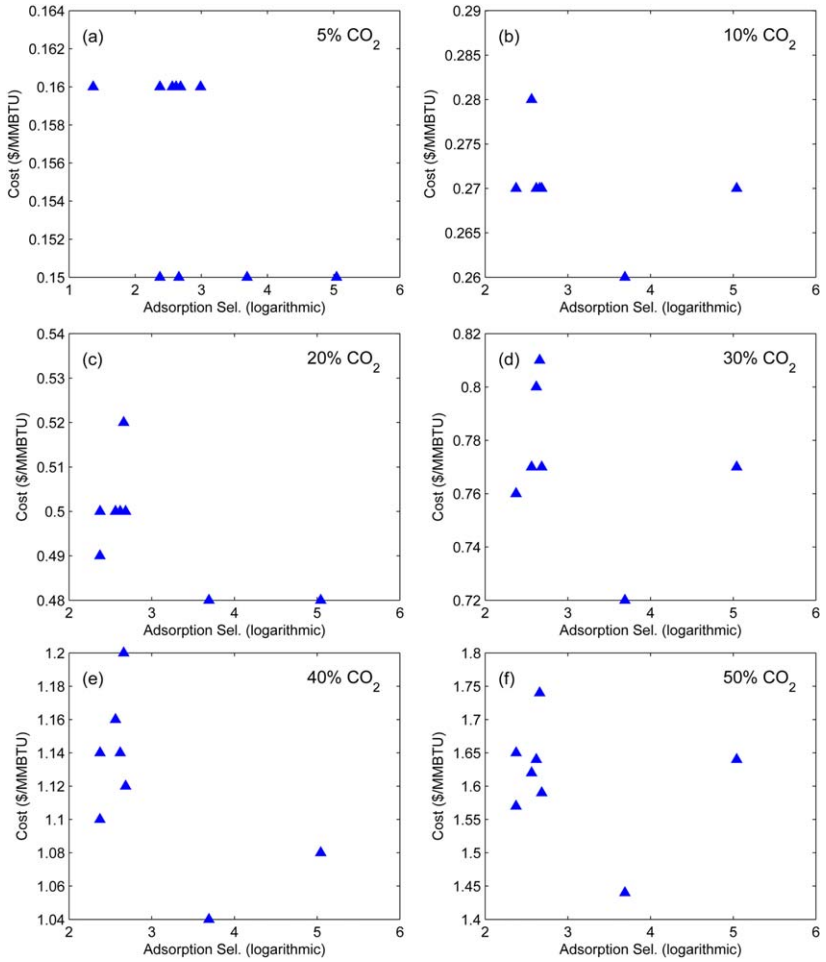

Figure 10. Plots of total cost vs. adsorption selectivity for each feed CO_2 composition.

(a) 5%, (b) 10%, (c) 20%, (d) 30%, (e) 40%, and (f) 50% CO_2. Each data point corresponds to a zeolite from Table 6, each of which satisfies purity and recovery constraints at the corresponding feed conditions. The lack of trends in these data indicates that adsorption selectivity is a poor predictor of cost. [Color figure can be viewed in the online issue, which is available at wileyonlinelibrary.com.]

except WEI.[52] It has been shown that each zeolite structure has an optimal Si/Al ratio for adsorbing CO_2 derived from a tradeoff between adsorption sites and pore volume.[54] This suggests that the performance of the top zeolites could be improved by allowing the introduction of cations.

Most literature screens materials for separations applications using adsorption selectivity as the sole metric, while ignoring the adsorption process and associated costs entirely. However, as we have previously demonstrated with CO_2/N_2 separation,[41] adsorption selectivity is not an appropriate predictor of cost. We confirm this finding for CH_4/CO_2 separation by detecting no significant correlation between adsorption selectivity and cost (see Figure 10). The fact that metrics such as adsorption selectivity (and heat of adsorption, saturation capacity, etc.) are independent of feed composition suggests that they cannot account for the difference in cost rankings between various feed compositions.

Conclusions

We have uncovered several cost-effective zeolites for adsorption-based separation of CH_4/CO_2 using a novel computational framework that combines material screening and process optimization. The hierarchical framework combines geometric-, atomistic-, and process-level modeling to screen a database of candidate zeolites and identify those feasible and economical for use in a PSA process. The *in silico* framework is applied to a diverse range of feed conditions, from 5 to 50% CO_2, representing the vast array of methane sources in the United States requiring purification. Many zeolites are incapable of achieving CH_4 with 97% purity and 95% recovery, though eight zeolites are identified that are feasible across all feed conditions considered. The separation can be achieved as economically as \$0.15/MMBTU from 5% CO_2 sources to \$1.44/MMBTU from 50% CO_2 sources, including the cost of CO_2 compression to 15 MPa for utilization and/or sequestration. These low costs are achieved using optimized process conditions, such as shorter columns and reduced pressures for adsorption and desorption.

Most of the zeolites studied are incapable of satisfying the stringent purity and recovery constraints necessary for natural gas purification. Starting from 199 possible zeolites, 26 are selected by screening metrics, and of these only eight are feasible for all feed CO_2 compositions. Particularly for methane sources more dilute in CO_2, these feasible zeolites have similar costs, providing flexibility in selecting a material based on potential commercial availability.

We demonstrate the necessity of applying a multiscale approach to identify the best materials and process configurations by showing no clear correlation between the overall cost

and material-centric metrics, such as adsorption selectivity. This is consistent with our recent findings for CO_2/N_2 separation.[41] The proposed approach and its associated technology opens the possibility for developing previously uneconomical energy sources including natural gas, coalbed methane, shale gas, enhanced oil recovery gas, biogas, and landfill gas sources.

Acknowledgments

This work was partially supported by the National Science Foundation under awards EFRI-0937706 and CBET-1263165. E.L.F. is also thankful for his National Defense Science and Engineering Graduate (NDSEG) fellowship. A portion of the computation was performed at the TIGRESS high performance computer center at Princeton University, which is jointly supported by the Princeton Institute for Computational Science and Engineering and the Princeton University Office of Information Technology.

Literature Cited

1. Cook PJ. *Clean Energy, Climate and Carbon*. London: CRC Press, 2012.
2. Baker RW, Lokhandwala K. Natural gas processing with membranes: an overview. *Ind Eng Chem Res*. 2008;47(7):2109–2121.
3. Tagliabue M, Farrusseng D, Valencia S, Aguado S, Ravon U, Rizzo C, Corma A, Mirodatos C. Natural gas treating by selective adsorption: material science and chemical engineering interplay. *Chem Eng J*. 2009;155(3):553–566.
4. Kidnay AJ, Parrish WR. *Fundamentals of Natural Gas Processing*. Boca Raton: CRC Press, 2006.
5. U.S. Energy Information Administration. Report Number DOE/EIA-0573(2009), 2011.
6. Bullin KA, Krouskop PE. Compositional variety complicates processing plans for US shale gas. *Oil Gas J*. 2009;107(10):50–55.
7. Zhong D-L, Ye Y, Yang C, Bian Y, Ding K. Experimental investigation of methane separation from low-concentration coal mine gas ($CH_4/N_2/O_2$) by tetra-n-butyl ammonium bromide semiclathrate hydrate crystallization. *Ind Eng Chem Res*. 2012;51(45):14806–14813.
8. Sircar S. Separation of methane and carbon dioxide gas mixtures by pressure swing adsorption. *Sep Sci Technol*. 1988;23(6–7):519–529.
9. Santos MPS, Grande CA, Rodrigues AE. Dynamic study of the pressure swing adsorption process for biogas upgrading and its responses to feed disturbances. *Ind Eng Chem Res*. 2013;52(15):5445–5454.
10. Mulgundmath V, Tezel F, Saatcioglu T, Golden T. Adsorption and separation of CO_2/N_2 and CO_2/CH_4 by 13X zeolite. *Can J Chem Eng*. 2012;90(3):730–738.
11. U.S. Energy Information Administration. Proved Reserves, Reserves Changes, and Production. U.S. Energy Information Administration, 2013. http://www.eia.gov/naturalgas/data.cfm. Accessed on December 20, 2013.
12. U.S. Environmental Protection Agency. Market Opportunities for Biogas Recovery Systems at U.S. Livestock Facilities. 2011. Available at: http://www.epa.gov/agstar/tools/market-oppt.html. Accessed on October 25, 2013.
13. U.S. Environmental Protection Agency. Energy Projects and Candidate Landfills. 2013. Available at: http://www.epa.gov/lmop/projects-candidates/index.html. Accessed on October 25, 2013.
14. Silva JA, Schumann K, Rodrigues AE. Sorption and kinetics of CO_2 and CH_4 in binderless beads of 13X zeolite. *Microporous Mesoporous Mater*. 2012;158:219–228.
15. Jensen NK, Rufford TE, Watson G, Zhang DK, Chan KI, May EF. Screening zeolites for gas separation applications involving methane, nitrogen, and carbon dioxide. *J Chem Eng Data*. 2012;57(1):106–113.
16. Delgado JA, Uguina MA, Sotelo JL, Ruiz B, Gomez JM. Fixed-bed adsorption of carbon dioxide/methane mixtures on silicalite pellets. *Adsorption*. 2006;12(1):5–18.
17. Bastin L, Barcia PS, Hurtado EJ, Silva JAC, Rodrigues AE, Chen B. A microporous metal-organic framework for separation of CO_2/N_2 and CO_2/CH_4 by fixed-bed adsorption. *J Phys Chem C*. 2008;112(5):1575–1581.
18. Keskin S, Sholl DS. Assessment of a metal-organic framework membrane for gas separations using atomically detailed calculations: CO_2, CH_4, N_2, H_2 mixtures in MOF-5. *Ind Eng Chem Res*. 2009;48(2):914–922.
19. Bae Y-S, Farha OK, Spokoyny AM, Mirkin CA, Hupp JT, Snurr RQ. Carborane-based metal-organic frameworks as highly selective sorbents for CO_2 over methane. *Chem Commun*. 2008;35:4135–4137.
20. Bae Y-S, Mulfort KL, Frost H, Ryan P, Punnathanam S, Broadbelt LJ, Hupp JT, Snurr RQ. Separation of CO_2 from CH_4 using mixed-ligand metal-organic frameworks. *Langmuir*. 2008;24(16):8592–8598.
21. Li J-R, Ma Y, McCarthy MC, Sculley J, Yu J, Jeong H-K, Balbuena PB, Zhou H-C. Carbon dioxide capture-related gas adsorption and separation in metal-organic frameworks. *Coord Chem Rev*. 2011;255(15–16):1791–1823.
22. Venna SR, Carreon MA. Highly permeable zeolite imidazolate framework-8 membranes for CO_2/CH_4 separation. *J Am Chem Soc*. 2010;132(1):76–78.
23. Pérez-Pellitero J, Amrouche H, Siperstein FR, Pirngruber G, Nieto-Draghi C, Chaplais G, Simon-Masseron A, Bazer-Bachi D, Peralta D, Bats N. Adsorption of CO_2, CH_4, and N_2 on zeolitic imidazolate frameworks: experiments and simulations. *Chem Eur J*. 2010;16(15):1560–1571.
24. Grande C, Blom R, Möller A, Möllmer J. High-pressure separation of CH_4/CO_2 using activated carbon. *Chem Eng Sci*. 2013;89:10–20.
25. Delgado JA, Uguina MA, Sotelo JL, Ruíz B, Rosário M. Carbon dioxide/methane separation by adsorption on sepiolite. *J Nat Gas Chem*. 2007;16(3):235–243.
26. Hart KE, Abbott LJ, McKeown NB, Colina CM. Toward Effective CO_2/CH_4 separations by sulfur-containing PIMs via predictive molecular simulations. *Macromolecules*. 2013;46(13):5371–5380.
27. Liu B, Smit B. Comparative molecular simulation study of CO_2/N_2 and CH_4/N_2 separation in zeolites and metal-organic frameworks. *Langmuir*. 2009;25(10):5918–5926.
28. Kim J, Abouelnasr M, Lin L-C, Smit B. Large-scale screening of zeolite structures for CO_2 membrane separations. *J Am Chem Soc*. 2013;135(20):7545–7552.
29. Keskin S, Sholl DS. Screening metal-organic framework materials for membrane-based methane/carbon dioxide separations. *J Phys Chem C*. 2007;111(38):14055–14059.
30. Kim J, Maiti A, Lin L-C, Stolaroff JK, Smit B, Aines RD. New materials for methane capture from dilute and medium-concentration sources. *Nat Commun*. 2013;4:1694.
31. Sircar S, Kumar R, Koch WR, VanSloun J. Recovery of methane from land fill gas. US Patent 4,770,676. 1988.
32. Kapoor A, Yang R. Kinetic separation of methane–carbon dioxide mixture by adsorption on molecular sieve carbon. *Chem Eng Sci*. 1989;44(8):1723–1733.
33. Olajossy A, Gawdzik A, Budner Z, Dula J. Methane separation from coal mine methane gas by vacuum pressure swing adsorption. *Chem Eng Res Des*. 2003;81(4):474–482.
34. Santos MP, Grande CA, Rodrigues AE. Pressure swing adsorption for biogas upgrading. Effect of recycling streams in pressure swing adsorption design. *Ind Eng Chem Res*. 2011;50(2):974–985.
35. Cavenati S, Grande CA, Rodrigues AE. Separation of $CH_4/CO_2/N_2$ mixtures by layered pressure swing adsorption for upgrade of natural gas. *Chem Eng Sci*. 2006;61(12):3893–3906.
36. Cavenati S, Grande CA, Rodrigues AE. Removal of carbon dioxide from natural gas by vacuum pressure swing adsorption. *Energy Fuels*. 2006;20(6):2648–2659.
37. Cavenati S, Grande CA, Rodrigues AE. Upgrade of methane from landfill gas by pressure swing adsorption. *Energy Fuels*. 2005;19(6):2545–2555.
38. Cavenati S, Grande CA, Rodrigues AE. Layered pressure swing adsorption for methane recovery from $CH_4/CO_2/N_2$ streams. *Adsorption*. 2005;11(1):549–554.
39. Grande CA, Rodrigues AE. Layered vacuum pressure-swing adsorption for biogas upgrading. *Ind Eng Chem Res*. 2007;46(23):7844–7848.
40. Spoorthi G, Thakur R, Kaistha N, Rao D. Process intensification in PSA processes for upgrading synthetic landfill and lean natural gases. *Adsorption*. 2011;17(1):121–133.
41. Hasan MMF, First EL, Floudas CA. Cost-effective CO_2 capture based on *in silico* screening of zeolites and process optimization. *Phys Chem Chem Phys*. 2013;15(40):17601–17618.
42. First EL, Gounaris CE, Wei J, Floudas CA. Computational characterization of zeolite porous networks: an automated approach. *Phys Chem Chem Phys*. 2011;13(38):17339–17358.
43. First EL, Floudas CA. MOFomics: computational pore characterization of metal-organic frameworks. *Microporous Mesoporous Mater*. 2013;165:32–39.

44. First EL, Gounaris CE, Wei J, Floudas CA. ZEOMICS. 2013. Available at: http://helios.princeton.edu/zeomics/. Accessed on October 25, 2013.
45. Gounaris CE, Floudas CA, Wei J. Rational design of shape selective separation and catalysis–I: concepts and analysis. *Chem Eng Sci*. 2006;61(24):7933–7948.
46. Gounaris CE, Wei J, Floudas CA. Rational design of shape selective separation and catalysis–II: mathematical model and computational studies. *Chem Eng Sci*. 2006;61(24):7949–7962.
47. Gounaris CE, Wei J, Floudas CA, Ranjan R, Tsapatsis M. Rational design of shape selective separations and catalysis: lattice relaxation and effective aperture size. *AIChE J*. 2009;56(3):611–632.
48. First EL, Gounaris CE, Floudas CA. Predictive framework for shape-selective separations in three-dimensional zeolites and metal–organic frameworks. *Langmuir*. 2013;29(18):5599–5608.
49. Haghpanah R, Majumder A, Nilam R, Rajendran A, Farooq S, Karimi IA, Amanullah M. Multi-objective optimization of a 4-step adsorption process for post-combustion CO_2 capture using finite volume technique. *Ind Eng Chem Res*. 2013;52(11):4249–4265.
50. Hasan MMF, Baliban RC, Elia JA, Floudas CA. Modeling, simulation and optimization of CO_2 capture for variable feed CO_2 concentration and feed flow. 2. Pressure swing adsorption and vacuum swing adsorption processes. *Ind Eng Chem Res*. 2012;51(48):15665–15682.
51. U.S. Energy Information Administration. Natural Gas Spot and Futures Prices. 2013. Available at: http://www.eia.gov/dnav/ng/ng_pri_fut_s1_m.htm. Accessed on October 25, 2013.
52. Baerlocher C, McCusker LB. Database of zeolite structures. Available at: http://www.iza-structure.org/databases/, Accessed on June 5, 2012.
53. Bushuev YG, Sastre G. Feasibility of pure silica zeolites. *J Phys Chem C*. 2010;114(45):19157–19168.
54. Lin L, Berger A, Martin R, Kim J, Swisher J, Jariwala K, Rycroft C, Bhown A, Deem M, Haranczyk M, Smit B. In silico screening of carbon-capture materials. *Nat. Mater*. 2012;11(7):633–641.
55. MCCCS Towhee. Available at: http://towhee.sourceforge.net/. Accessed on January 25, 2012.
56. García-Pérez E, Parra J, Ania C, García-Sánchez A, van Baten J, Krishna R, Dubbeldam D, Calero S. A computational study of CO_2, N_2, and CH_4 adsorption in zeolites. *Adsorption*. 2007;13:469–476.
57. Ruthven DM. *Principles of Adsorption and Adsorption Processes*. New York: Wiley, 1984.
58. Uppaluri RVS, Linke P, Kokossis AC. Synthesis and optimization of gas permeation membrane networks. *Ind Eng Chem Res*. 2004;43(15):4305–4322.
59. Hasan MMF, Baliban RC, Elia JA, Floudas CA. Modeling, simulation and optimization of CO_2 capture for variable feed CO_2 concentration and feed flow. 1. Chemical absorption and membrane processes. *Ind Eng Chem Res*. 2012;51(48):15642–15664.
60. Seider WD, Seader JD, Lewin DR, Widagdo S. *Product and Process Design Principles: Synthesis, Analysis, and Evaluation*. New York: Wiley, 2004.
61. Fisher KS, Searcy K, Rochelle GT, Ziaii S, Schubert C. Advanced amine solvent formulations and process integration for near-term CO_2. Capture success.DE-FG02–06ER84625. US Department of Energy, 2007. http://www.netl.doe.gov/research/coal/carbon-capture/post-combustion/adv-amine. Accessed on December 20, 2013.
62. Jones DR, Schonlau M, Welch WJ. Efficient global optimization of expensive black-box functions. *J Global Optim*. 1998;13(4):455–492.

Appendix A: GCMC Simulations

To calculate adsorption isotherms and heat of adsorption, we employ the GCMC method implemented in the software package MCCCS Towhee[55] using the silica zeolite force field by García-Pérez et al.[56] Single-component adsorption isotherms for CO_2 and CH_4 are calculated at five temperatures, $T_p = (298, 323, 348, 373, \text{and } 398\ K)$, with data points collected at 14 pressures, $N_p = (1.3, 2.7, 5.3, 10.7, 16.0, 21.3, 42.7, 85.3, 101.3, 133.3, 266.6, 666.6, 1333.2, \text{and } 2666.4\ kPa)$. The configuration of the GCMC simulations is described in Hasan et al.,[41] and is summarized below.

Lennard-Jones parameters and partial charges are provided in Table A1. Nonbonded interactions are cutoff at 1.2 nm, and the potential is shifted. A hard inner cutoff distance of 0.07 nm is used. The electrostatic potential is Coulomb-style with Ewald summations and kmax fixed to 5 and kalp set to 5.6. Blocking spheres, which are generated from the ZEOMICS[42,44] pore characterizations, prevent insertions to inaccessible pores. Each simulation to calculate one (T, P) sample point is run for 1,000,000 equilibration moves and 1,000,000 production moves. A linear regression model is used to calculate heat of adsorption from the potential energies.

Table A1. Lennard-Jones Parameters from the Force Field for Silica Zeolites by García-Pérez et al.[56]

	ϵ/k_B (K)	σ (nm)
O_{zeo}—C	50.2	0.27815
O_{zeo}—O_{CO_2}	84.93	0.29195
O_{zeo}—CH_4	115	0.347
C—C	28.129	0.276
C—O_{CO_2}	47.59	0.289
O_{CO_2}—O_{CO_2}	80.507	0.3033
CH_4—CH_4	158.5	0.372

CH_4 Utilizes a United Atom Model. Partial charges (e^-): $O_{zeo} = -1.025$, $C = +0.6512$, $O_{CO_2} = -0.3256$.

The adsorption isotherms are fit to a dual-site Langmuir model as follows. The predicted molar loading, $q_{i,z}^{*,\text{theo}}$, of component i in zeolite z is given by

$$q_{i,z}^{*,\text{theo}} = \sum_{s=1}^{2} \frac{q_{i,s,z}^{\text{sat}} b_{i,s,z} p_i}{1 + \sum_i b_{i,s,z} p_i} \quad \forall (i,z) \tag{A1}$$

where $q_{i,s,z}^{\text{sat}}$ is the saturation loading of component i at site s of zeolite z. Two adsorption sites are available for both CO_2 and CH_4. The parameter $b_{i,s,z}$ in Eq. A1 has an Arrhenius-type temperature dependence given by

$$b_{i,s,z} = \frac{b_{i,s,z}^{o} e^{-\frac{\Delta U_{i,s,z}}{RT}}}{RT} \quad \forall (i,s,z) \tag{A2}$$

The isotherm parameters $q_{i,s,z}^{\text{sat}}, b_{i,s,z}^{o}$, and $\Delta U_{i,s,z}$ are found by minimizing the root mean square error (RMSE) between the data points generated by GCMC and the Langmuir model with appropriate weights

$$\text{MIN RMSE} = \sqrt{\sum_{i \in CO_2, CH_4} \sum_{n \in N_p} \sum_{t \in T_p} \left(\frac{q_{i,n,t}^{*,\text{theo}} - q_{i,n,t}^{*}}{\max_{n' \in N_p} q_{i,n',t}^{*}} \right)^2} \tag{A3}$$

where $q_{i,n,t}^{*,\text{theo}}$ is the predicted equilibrium solid loading from Eq. A1, and $q_{i,n,t}^{*}$ is the equilibrium solid loading calculated by GCMC.

Appendix B: NAPDE Model of the PSA Process

The adsorption process is simulated using an NAPDE model.

The indices, sets, parameters, variables, and equations that define this model are described below.

We use the following indices:

i : component

n : packed column

l : bed length

t : time

We define the following set of components.

$$i \in I = \{CO_2, CH_4\}$$

The following parameters are used in the NAPDE model:

F : feed flow rate

$y_{i,f}$: mole fraction of component i in the feed gas

T_o : feed temperature

P_f : feed flow rate

u_o : feed velocity

T_a : outside air temperature

$y_{i,0}$: initial mole fraction of component i in the bed

P_{atm} : atmospheric pressure

K_z : effective heat conductivity

K_w : thermal heat conductivity of column wall

h_{in} : heat-transfer coefficient inside the column

h_o : heat-transfer coefficient for outside the column

C_{pw} : specific heat capacity of column wall

C_{pg} : specific heat capacity of gas mixture

C_{pa} : specific heat capacity of adsorbed gas in solid

C_{ps} : specific heat capacity of adsorbent

R : gas constant

q_s : saturation capacity

b_i^o : isotherm parameter for component i

ΔU_i : heat of adsorption for component i

τ_p : tortuosity factor

D_M : molecular diffusivity of CO_2-CH_4 mixture

D_p : macropore diffusivity, $D_p = \dfrac{D_M}{\tau_p}$

UC : unit operating cost

d_p : particle diameter

r_p : particle radius, $\dfrac{d_p}{2}$

ε_p : particle porosity

ε : bed porosity

ρ_w : density of column

ρ_s : density of solid particle

μ : gas viscosity

ϕ : annualization factor

α : unit capital cost

β : exponent of power cost

k_p : bed permeability defined by the correlation

: $k_p = \dfrac{d_p^2}{150}\left(\dfrac{\varepsilon}{1-\varepsilon}\right)^2$

The performance of the PSA process depends on the following decision variables:

N : number of columns

P_{ads} : highest pressure of the system

L : column length

D : column diameter

P_{des} : desorption pressure

t_{pr} : duration of the pressurization step, 20 s

t_{ads} : duration of the adsorption step

t_{des} : duration of the desorption step

γ : binary variable indicating method of feed expansion

Depending on the values selected for the above decision variables, the following system variables can vary along the column length (l) and over time (t):

$P(l,t)$: pressure inside the column

$T(l,t)$: temperature inside the column

$T_W(l,t)$: column wall temperature

$u_z(l,t)$: velocity

$c_i(l,t)$: concentration of component i in the gas phase

$y_i(l,t)$: mole fraction of component i in the gas phase

$x_i(l,t)$: fractional loading of component i in the solid phase

$x_i^*(l,t)$: equilibrium fractional loading of component i in the solid phase

$k_i(l,t)$: mass-transfer coefficient of component i

$b_i(l,t)$: temperature dependent parameter for component i

$B_i(l,t)$: isotherm parameter for component i

$-\Delta H_i(l,t)$: change in internal energy for component i

$\rho_g(l,t)$: density of gas obtained from the ideal gas law

The following dimensionless variables are used to describe the adsorption/desorption process inside a column

$$\begin{aligned} &\bar{P} = \frac{P}{P_{ads}};\ \bar{P}_{des} = \frac{P_{des}}{P_{ads}};\ \bar{T} = \frac{T}{T_0};\ \bar{T}_w = \frac{T_w}{T_0};\ \bar{T}_a = \frac{T_a}{T_0};\\ &x_i = \frac{\bar{q}_i}{q_s};\ x_i^* = \frac{q_i^*}{q_s};\ \bar{u}_z = \frac{u_z}{u_0};\ Z = \frac{l}{L};\ \tau = \frac{tu_o}{L} \end{aligned} \tag{B1}$$

Adsorption/desorption model

The following component mass balances are used to calculate the CO_2 mole fraction in the gas phase

$$\begin{aligned} &\frac{\partial y_i}{\partial \tau} = \frac{1}{Pe}\left(\frac{\partial^2 y_i}{\partial Z^2} + 1\bar{P}\frac{\partial y_i}{\partial Z}\frac{\partial \bar{P}}{\partial Z} - 1\bar{T}\frac{\partial y_i}{\partial Z}\frac{\partial \bar{T}}{\partial Z}\right)\\ &-\bar{u}_z\frac{\partial y_i}{\partial Z} + \psi\bar{T}\bar{P}\left((y_i - 1)\frac{\partial x_i}{\partial \tau} + y_i\frac{\partial x_{CH_4}}{\partial \tau}\right) \quad \forall i | (i = CO_2) \end{aligned} \tag{B2}$$

where $\psi = \left(\frac{1-\varepsilon}{\varepsilon}\frac{RT_o q_s}{P_{ads}}\right)$, and $Pe = \frac{u_o L}{D_L}$ is the Peclet number. To define the y_i variables as mole fractions, the following constraint is required

$$\sum_i y_i = 1 \tag{B3}$$

The overall mass balance is given by

$$\frac{\partial \bar{P}}{\partial \tau} - \bar{P}\bar{T}\frac{\partial \bar{T}}{\partial \tau} = \left(-\bar{P}\frac{\partial \bar{u}_z}{\partial Z} - \bar{u}_z\frac{\partial \bar{P}}{\partial Z} + \bar{u}_z\bar{P}\bar{T}\frac{\partial \bar{T}}{\partial Z}\right) - \bar{T}\psi\frac{\partial}{\partial \tau}\left(\sum_i x_i\right) \tag{B4}$$

Darcy's law is used to compute the dimensionless interstitial gas velocity as follows

$$\bar{u}_z = -\left(\frac{k_p P_{ads}}{\mu u_o L}\right)\frac{\partial \bar{P}}{\partial Z} \tag{B5}$$

To allow heat transfer across the column wall, we have

$$\frac{\partial \bar{T}_w}{\partial \tau} = \pi_1 \frac{\partial^2 \bar{T}_w}{\partial Z^2} + \pi_2(\bar{T} - \bar{T}_w) - \pi_3(\bar{T}_w - \bar{T}_a) \tag{B6}$$

where

$$\pi_1 = \frac{K_w}{\rho_w C_{pw} u_o L} \tag{B7a}$$

$$\pi_2 = \frac{2 r_i h_{in} L}{\rho_w C_{pw} u_o \left(r_o^2 - r_{in}^2\right)} \tag{B7b}$$

$$\pi_3 = \frac{2 r_o h_o L}{\rho_w C_{pw} u_o \left(r_o^2 - r_{in}^2\right)} \tag{B7c}$$

with r_{in} and r_o being the inside and outside radii of the packed column, respectively.

An energy balance is used to calculate the temperature inside the column as follows

$$\frac{\partial \bar{T}}{\partial \tau} = \pi_4 \frac{\partial^2 \bar{T}}{\partial Z^2} - \pi_5 \bar{u}_z \frac{\partial \bar{T}}{\partial Z} + \sum_{i=1}^{N} (\pi_{6i} + \pi_7 \bar{T}) \frac{\partial x_i}{\partial \tau} - \pi_8(\bar{T} - \bar{T}_w) \tag{B8}$$

where

$$\pi_4 = \frac{K_z}{\varepsilon\left(\rho_g C_{pg} + \frac{1-\varepsilon}{\varepsilon}\left(\rho_s C_{ps} + C_{pa} q_s\right)\right) u_o L} \tag{B9a}$$

$$\pi_5 = \frac{\rho_g C_{pg}}{\left(\rho_g C_{pg} + \frac{1-\varepsilon}{\varepsilon}\left(\rho_s C_{ps} + C_{pa} q_s\right)\right)} \tag{B9b}$$

$$\pi_{6i} = \frac{\frac{1-\varepsilon}{\varepsilon}(-\Delta H_i) q_s}{T_0\left(\rho_g C_{pg} + \frac{1-\varepsilon}{\varepsilon}\left(\rho_s C_{ps} + C_{pa} q_s\right)\right)} \tag{B9c}$$

$$\Delta H_i = \Delta U_i - RT \tag{B9d}$$

$$\pi_7 = \frac{\frac{1-\varepsilon}{\varepsilon}(C_{pg} - C_{pa}) T_0 q_s}{T_0\left(\rho_g C_{pg} + \frac{1-\varepsilon}{\varepsilon}\left(\rho_s C_{ps} + C_{pa} q_s\right)\right)} \tag{B9e}$$

$$\pi_8 = \frac{2 h_{in} L}{\varepsilon r_i u_o \left(\rho_g C_{pg} + \frac{1-\varepsilon}{\varepsilon}\left(\rho_s C_{ps} + C_{pa} q_s\right)\right)} \tag{B9f}$$

We use a linear driving force model to describe the mass transfer

$$\frac{\partial x_i}{\partial \tau} = \frac{k_i L}{u_o}(x_i^* - x_i) \quad \forall i \tag{B10}$$

We use the following dual-site Langmuir model to compute x_i^*

$$x_i^* = \sum_{s=1}^{2} \frac{\left(\frac{q_{i,s}^{sat}}{q_s}\right) b_{i,s} c_i}{1 + \sum_i b_{i,s} c_i} \quad \forall i \tag{B11}$$

where $q_{i,s}^{sat}$ is the saturation loading of component i at site s ($s = 1,2$). The temperature dependent parameter $b_{i,s}$ is calculated by the following Arrhenius-type expression

$$b_{i,s} = \frac{b_{i,s}^o e^{-\frac{\Delta U_{i,s}}{RT}}}{RT} \quad \forall (i,s) \tag{B12}$$

Equations B1–B12 constitute the adsorption/desorption model in an adsorbent-packed column. To complete the PSA cycle with three steps, we also need appropriate boundary and initial conditions which we describe below.

PSA cycle formulation: Initial and boundary conditions

Pressurization. The initial conditions for the first pressurization step are

$$\begin{aligned} y_i &= y_{i,0} \\ \bar{P} &= \bar{P}_{des} \\ \bar{T} &= 1 \\ x_i &= x_i^*|_{y_{i,0}} \end{aligned} \tag{B13}$$

Initial conditions for each subsequent step are the final conditions of the previous step due to the cyclic process. Therefore, initial conditions for the remaining steps are unspecified.

Boundary conditions are applied at the ends of the adsorption column, which are positioned at $Z = 0^+$ and $Z = 1^-$ The boundary conditions at $Z = 0^+$ and $Z = 1^-$ for the pressurization step are given by Eqs. B14 and B15, respectively

$$\begin{aligned} \frac{1}{Pe}\frac{\partial y_i}{\partial Z} &= -\bar{u}_z(y_{i,f} - y_i) \\ \frac{1}{Pe_H}\frac{\partial \bar{T}}{\partial Z} &= -\bar{u}_z(1 - \bar{T}) \\ \bar{T}_w &= \bar{T}_a \\ \bar{P} &= f(\tau); \quad \bar{P}_{des} \rightarrow 1 \end{aligned} \tag{B14}$$

$$\begin{aligned} \frac{\partial y_i}{\partial Z} &= 0 \\ \frac{\partial \bar{T}}{\partial Z} &= 0 \\ \bar{T}_w &= \bar{T}_a \\ \frac{\partial \bar{P}}{\partial Z} &= 0 \end{aligned} \tag{B15}$$

Adsorption. The boundary conditions at $Z = 0^+$ and $Z = 1^-$ for the adsorption step are given by Eqs. B16 and B17, respectively

$$\begin{aligned} \frac{\partial y_i}{\partial Z} &= -Pe(y_{i,f} - y_i) \\ \frac{1}{Pe_H}\frac{\partial \bar{T}}{\partial Z} &= -(1 - \bar{T}) \\ \bar{T}_w &= \bar{T}_a \\ \bar{P} &= 1 + \frac{\Delta}{P_{ads}} \end{aligned} \tag{B16}$$

$$\begin{aligned} \frac{\partial y_i}{\partial Z} &= 0 \\ \frac{\partial \bar{T}}{\partial Z} &= 0 \\ \bar{T}_w &= \bar{T}_a \\ \bar{P} &= 1 \end{aligned} \tag{B17}$$

where $Pe_H = \frac{\varepsilon u_o L \rho_g C_{pg}}{K_z}$.

Desorption. The boundary conditions at $Z=0^+$ and $Z=1^-$ for the desorption step are given by Eqs. B18 and B19, respectively

$$\begin{aligned}\frac{\partial y_i}{\partial Z}&=0\\ \frac{\partial \bar{T}}{\partial Z}&=0\\ \bar{T}_{\mathrm{w}}&=\bar{T}_{\mathrm{a}}\\ \frac{\partial \bar{P}}{\partial Z}&=0\end{aligned} \tag{B18}$$

$$\begin{aligned}\frac{\partial y_i}{\partial Z}&=0\\ \frac{\partial \bar{T}}{\partial Z}&=0\\ \bar{T}_{\mathrm{w}}&=\bar{T}_{\mathrm{a}}\\ \bar{P}&=f(\tau):\bar{P}_{\mathrm{ads}}\rightarrow\bar{P}_{\mathrm{des}}\end{aligned} \tag{B19}$$

Design specifications

In a PSA process, the adsorption pressure must be greater than the desorption pressure. This is captured by the following constraint

$$P_{\mathrm{ads}}\geq P_{\mathrm{des}} \tag{B20}$$

The other important design specifications are the desired purity and recovery of CH_4. The pipeline specification for the transportation of natural gas requires that the CH_4 must be at least 97% pure. The following constraint ensures that the minimum CH_4 purity (Pu) obtained from the process is 97%

$$\mathrm{Pu}=\frac{\int_o^{t_{\mathrm{ads}}}\bar{u}_z y_{\mathrm{CH_4}}\frac{\bar{P}}{RT}dt|_{Z=1^-}}{\sum_i\int_o^{t_{\mathrm{ads}}}\bar{u}_z y_i\frac{\bar{P}}{RT}dt|_{Z=1^-}}\geq 0.97 \tag{B21}$$

It is also desirable to recover as much CH_4 as possible. To ensure that at least 95% of the CH_4 in the feed is recovered as product, we impose the following constraint on recovery (Re)

$$\mathrm{Re}=\frac{\int_o^{t_{\mathrm{ads}}}\bar{u}_z y_{\mathrm{CH_4}}\frac{\bar{P}}{RT}dt|_{Z=1^-}}{\int_o^{t_{\mathrm{pr}}}\bar{u}_z y_{\mathrm{CH_4}}\frac{\bar{P}}{RT}dt|_{Z=0^+}+\int_o^{t_{\mathrm{ads}}}\bar{u}_z y_{\mathrm{CH_4}}\frac{\bar{P}}{RT}dt|_{Z=0^+}}\geq 0.95 \tag{B22}$$

Each column is identical and receives equal amount of feed in each cycle. The number of columns, N, is selected such that the idle times for the two vacuum pumps are minimized for maximum capacity utilization. This is achieved by selecting N to be the rounded-down integer value of the fraction $t_c/t_{\max}$, where t_c is the total cycle duration and $t_{\max}$ is the longest step duration. These are defined formally as follows

$$t_c=t_{\mathrm{pr}}+t_{\mathrm{ads}}+t_{\mathrm{des}} \tag{B23}$$

$$t_{\max}=\max\left[t_{\mathrm{pr}},t_{\mathrm{ads}},t_{\mathrm{des}}\right] \tag{B24}$$

Additional columns would require additional vacuum pumps, which is not permitted in our model.

The inner diameter of each column, D, is calculated by assuming that the flow rate to the adsorption step is much larger than the flow rate to the pressurization step and, therefore, defines the column rating. It is calculated by

$$D=\sqrt{\frac{4}{\pi}\times\left(\frac{P_{\mathrm{atm}}}{P_{\mathrm{ads}}}\times\frac{T_o}{273.15}\times 22.4\right)\times\left(\frac{F\times t_c}{u_o\times t_{\mathrm{ads}}\times N}\right)} \tag{B25}$$

Investment cost calculations

The total investment cost, TIC, is calculated as the sum of investment costs for all compressors, expanders, columns, and vacuum pumps present in the PSA process by the following

$$\begin{aligned}\mathrm{TIC}=&\alpha_c\left(\bar{W}_{\mathrm{f,comp}}\right)^{\beta_c}+\alpha_e\left(\bar{W}_{\mathrm{f,exp}}\right)^{\beta_e}\gamma+\alpha_v\left(\bar{W}_{\mathrm{des}}\right)^{\beta_v}\\ &+\alpha_c\left(\bar{W}_{\mathrm{p,comp}}\right)^{\beta_c}+\alpha_c\left(\bar{W}_{\mathrm{seq}}\right)^{\beta_c}+\alpha_{\mathrm{he}}\left(\bar{W}_{\mathrm{cool}}\right)^{\beta_{\mathrm{he}}}+\sum_n \mathrm{PC}_n\end{aligned} \tag{B26}$$

Here, the investment cost of an equipment is considered to be a function of its rating or size, and the cost parameters α and β, which are obtained from literature.[50,58,59] The binary variable γ is used to determine whether an expansion turbine or pressure relief valve is selected depending on the economic tradeoff, and it is defined subsequently. The rating calculations are presented below.

$\bar{W}_{\mathrm{f,comp}}$ and $\bar{W}_{\mathrm{f,exp}}$ are the horsepower ratings of the feed compressor and expander, respectively, and are calculated using the following expressions

$$\bar{W}_{\mathrm{f,comp}}=\begin{cases}\frac{1}{\eta}\times F\times\frac{8314}{746}\times T_o\times\frac{\gamma}{\gamma-1}\left[\left(\frac{P_{\mathrm{ads}}}{P_{\mathrm{f}}}\right)^{\frac{\gamma-1}{\gamma}}-1\right] & \text{if } P_{\mathrm{ads}}\geq P_{\mathrm{f}}\\ 0 & \text{if } P_{\mathrm{ads}}<P_{\mathrm{f}}\end{cases} \tag{B27}$$

and

$$\bar{W}_{\mathrm{f,exp}}=\begin{cases}\eta\times F\times\frac{8314}{746}\times T_o\times\frac{\gamma}{\gamma-1}\left[1-\left(\frac{P_{\mathrm{ads}}}{P_{\mathrm{f}}}\right)^{\frac{\gamma-1}{\gamma}}\right] & \text{if } P_{\mathrm{ads}}<P_{\mathrm{f}}\\ 0 & \text{if } P_{\mathrm{ads}}\geq P_{\mathrm{f}}\end{cases} \tag{B28}$$

The average horsepower rating of the desorption vacuum pump is W_{des}, which is given by

$$\bar{W}_{\mathrm{des}}=\frac{W_{\mathrm{des}}}{t_{\mathrm{des}}\times 746} \tag{B29}$$

where

$$W_{\mathrm{des}}=\frac{1}{\eta}\varepsilon\pi D^2 u_0 P_{\mathrm{ads}}\frac{\gamma}{\gamma-1}\int_o^{t_{\mathrm{des}}}\left(\bar{u}_z\bar{P}|_{Z=0}\right)\left[\left(\frac{P_{\mathrm{atm}}}{P_{\mathrm{ads}}\bar{P}|_{Z=0}}\right)^{\frac{\gamma-1}{\gamma}}-1\right]dt \tag{B30}$$

For an average mass flow rate, $\bar{M}_{\mathrm{des}}$, through the desorption vacuum pump, $\bar{W}_{\mathrm{seq}}$ and $\bar{W}_{\mathrm{cool}}$ represent the total compression power and the cooling duty of the six-stage CO_2 compression train. These values are given by

$$\bar{W}_{\mathrm{seq}}=\frac{6}{\eta}\bar{M}_{\mathrm{des}}\frac{8314}{746}\times T_{\mathrm{atm}}\frac{\gamma}{\gamma-1}\left[(2.3)^{\frac{\gamma-1}{\gamma}}-1\right] \tag{B31}$$

and

$$\bar{W}_{\text{cool}} = 6 \times \bar{M}_{\text{des}} \times C_{\text{pg}} \left[(2.3)^{\frac{\gamma-1}{\gamma}} - 1 \right] \times T_{\text{atm}} \tag{B32}$$

Finally, the purchase cost, PC_n, of each column n is calculated as follows[60]

$$\text{PC}_n = F_{\text{M}} C_{\text{V},n} + C_{\text{PL},n} + V_{\text{P},n} C_{\text{PK}} + C_{\text{DR},n} \tag{B33}$$

where F_{M} is the factor for materials-of-construction, $C_{\text{V},n}$ is the free-on-board purchase cost of the empty vessel with weight W_n,$C_{\text{PL},n}$ is the cost of adsorber platforms and ladders, $V_{\text{P},n}$ is the adsorber packing volume, C_{PK} is the installed cost of the packing for unit volume, and $C_{\text{DR},n}$ is the installed cost of flow distributors and redistributors for column n. These are calculated by the following expressions

$$C_{\text{V},n} = \exp\left\{ 7.2756 + 0.18255 \ln(W_n) + 0.02297 [\ln(W_n)]^2 \right\} \tag{B34}$$

$$W_n = \pi (39.37 D_n + t_{\text{S}}) [39.37 (0.8 D_n + L_n)] t_{\text{S}} \rho \tag{B35}$$

$$C_{\text{PL},n} = 300.9 (3.281 D_n)^{0.63316} (3.281 L_n)^{0.80161} \tag{B36}$$

$$V_{\text{P},n} = \frac{\pi}{4} (3.281 D_n)^2 (3.281 L_n) \tag{B37}$$

$$C_{\text{DR},n} = 3 \times 125 \times \frac{\pi}{4} (3.281 D_n)^2 \tag{B38}$$

where L_n and D_n are the length and diameter of column n, t_{S} is the shell thickness, and ρ is the density of the carbon steel. We use $F_{\text{M}} = 2.1$, $C_{\text{PK}} = 40$, $\rho = 0.284$ lb/in.^{3}, and $t_{\text{S}} = 2$ in.[60]

Operating cost calculations

The annual operating time is taken to be 8000 h. The feed and product compressors and the desorption vacuum pump require electricity, while the feed expander, if present, provides electricity. Therefore, the net annual operating cost (AOC) for these units is given by

$$\begin{aligned} \text{AOC}_{\text{cap}} &= (0.746 \times 800) \times \text{UCE} \\ &\times \left[\bar{W}_{\text{f,comp}} - \bar{W}_{\text{f,exp}} \gamma + N \times \bar{W}_{\text{des}} + \bar{W}_{\text{p,comp}} \right] \end{aligned} \tag{B39}$$

where UCE is the price of electricity, which is taken to be \$0.07/kWh. The binary variable γ indicates the feed expansion method, and it is defined subsequently.

The multistage compression train for CO_2 sequestration has the following operating costs

$$\text{AOC}_{\text{seq}} = (0.746 \times 800) \times \left[\text{UCE} \times \bar{W}_{\text{seq}} + \text{UCCW} \times \bar{W}_{\text{cool}} \right] \tag{B40}$$

where UCCW is the price of cooling water used in the intercoolers, which is taken to be \$1/ton.

The operating costs also include the yearly purchase and replacement costs of the zeolite sorbent. These costs are dependent on the volume of material required, and is calculated by

$$\text{AOC}_{\text{mat}} = \text{UCM} \times \frac{\pi}{4} D^2 L N \rho_{\text{s}} \tag{B41}$$

where UCM is the price for sorbent purchase and replacement, which is taken to be \$2/kg.

From these expressions, the total AOC is given by

$$\text{AOC} = \text{AOC}_{\text{cap}} + \text{AOC}_{\text{seq}} + \text{AOC}_{\text{mat}} \tag{B42}$$

Feed expansion

The feed can be expanded with either an expansion turbine or a pressure relief valve. An expansion turbine produces electricity that reduces operating costs, but it requires additional investment cost. The pressure relief valve produces no electricity but has negligible cost. There is a tradeoff between the investment cost and operating revenue of an expansion turbine that determines which feed expander should be selected. The binary variable γ, which depends on the feed flow rate and adsorption pressure as illustrated in Figure 9, is defined as

$$\gamma = \begin{cases} 1 & \text{if } \phi \alpha_e \left(\bar{W}_{\text{f,exp}} \right)^{\beta_e} < (0.746 \times 800) \times \text{UCE} \times \bar{W}_{\text{f,exp}} \\ 0 & \text{otherwise} \end{cases} \tag{B43}$$

where a value of 1 indicates that the expansion turbine is selected, and a value of 0 indicates that the pressure relief valve is selected. The annualizing factor, ϕ, is discussed below.

Objective function

The objective is to minimize the total cost of CH_4 recovery and CO_2 capture and compression per unit energy content of the recovered CH_4 (million BTU = MMBTU). To formulate the objective, we first derive the total annualized cost TAC (\$/yr) of the PSA process

$$\text{TAC} = [\phi \text{TIC} + \text{AOC}] \tag{B44}$$

where the annualizing factor, ϕ, is a function of the capital recovery factor (taken to be 0.154), the total plant cost, and the annual maintenance cost (taken to be 5% of the total plant cost). The total plant cost includes the total equipment installed costs, the indirect cost (taken to be 32% of the total installed cost), and the balance of plant cost (taken to be 20% of the total installed cost). The installed cost of a piece of equipment includes the purchase and installation costs. The installation costs are taken to be 4% of the purchase costs for general equipment (columns and heat exchangers) and 80% of the purchase costs for movers (compressors and vacuum pumps).[61]

TAC is converted to \$/MMBTU, TC_{MMBTU}, which is minimized

$$\begin{aligned} &\text{MIN } TC_{\text{MMBTU}} (\$/\text{MMBTU}) \\ &= \left[\frac{TAC}{8000 \times 3600} \times \frac{1}{F \times y_{\text{CH}_4,\text{f}} \times Re} \times \frac{10^3}{MW_{\text{CH}_4} \times EC_{\text{CH}_4}} \right] \end{aligned} \tag{B45}$$

where F is the feed flow rate (kmol/s), $y_{\text{CH}_4,\text{f}}$ is the feed CH_4 composition, Re is the CH_4 recovery as defined by 32, $MW_{\text{CH}_4} = 16.04$ g/mol is the molecular weight of CH_4, and EC_{CH_4} is the energy content (52.63 MMBTU/ton) of CH_4.

Equations B1–B45 define the NAPDE model for the PSA process optimization. The model includes five major independent variables, namely column length (L), adsorption pressure (P_{ads}), desorption pressure (P_{des}), and the step durations for adsorption (t_{ads}) and desorption (t_{des}).

Appendix C: Grey-Box Constrained Optimization Model of the PSA Process

To optimize the NAPDE model in a grey-box constrained optimization framework, the NAPDE model is discretized in space and time and evaluated for various combinations of the input variables, each denoted as a sample. Based on the input–output data generated from these samples, a Kriging-based surrogate model is constructed to approximate the NAPDE model. The indices, sets, parameters, variables, and equations that define the surrogate model are described below.

Sets

The following sets are defined with their corresponding indices

$i, i', \text{or} j \in S$: set of sample points

$k \in K$

$=\{L, P_{\text{ads}}, P_{\text{des}}, t_{\text{ads}}, t_{\text{des}}\}$: set of input (decision) variables

$m \in M$

$=\{\text{purity, recovery, cost}\}$: set of output (response) variables

Sampling inputs

$x_{i,k}$: value of input variable k at sample i

$y_{i,m}$: value of the output variable m at sample i

Kriging parameters

μ_m : average (mean) of output m

$\theta_{k,m}$: weight assigned to input k for output m

Variables

x_k^* : a new value of the input variable k

y_m^* : interpolated output variable m corresponding to x_k^*

Equations

The Kriging model postulates the following input–output relation between $y_{i,m}$ and $x_{i,k}$

$$y_{i,m}=\mu_m+\sum_{j\in S} c_{j,m}u_{i,j,m} \quad i \in S, m \in M \tag{C1}$$

In Eq. C1, an exponential correlation of the weighted distance is used as the basis function, $u_{i,j,m}$, which is defined as follows

$$u_{i,j,m}=\exp\left[-\sum_k \theta_{k,m}\left(x_{i,k}-x_{j,k}\right)^2\right] \quad i \in S, j \in S, m \in M \tag{C2}$$

Here, μ_m and $\theta_{k,m}$ are parameters that are fit to the samples. One advantage of using an exponential correlation of the distances is that for exact interpolation, $c_{i,m}$ and $v_{i,j,m}$ take the following explicit forms[62]

$$c_{i,m}=\sum_{j\in S} v_{i,j,m}\left(y_{j,m}-\mu_m\right) \quad i \in S, m \in M \tag{C3}$$

and

$$\sum_{i'\in S} u_{i,i',m}v_{i',j,m}=I_{i,j,m} \quad i \in S, j \le i, m \in M \tag{C4}$$

where I is the identity matrix.

Now, for a new point in the sampling space, x_k^*, we predict the output, y_m^*, from the above Kriging model based on $x_{i,k}$ and $y_{i,m}$ data as follows

$$y_m^*=\mu_m+\sum_{i\in S} c_{i,m}\exp\left[-\sum_k \theta_{k,m}\left(x_k^*-x_{i,k}\right)^2\right] \quad i \in S, m \in M \tag{C5}$$

Therefore, the following NLP model is the surrogate model used for process optimization

$$\text{MIN } y_{\text{cost}}^* \tag{C6}$$

subject to

$$y_m^*=\mu_m+\sum_{i\in S} c_{i,m}\exp\left[-\sum_k \theta_{k,m}\left(x_k^*-x_{i,k}\right)^2\right] \quad i \in S, m \in \{\text{purity, recovery, cost}\} \tag{C7}$$

$$y_{\text{purity}}^* \ge 0.97 \tag{C8}$$

$$y_{\text{recovery}}^* \ge 0.95 \tag{C9}$$

$$x_{k=P_{\text{ads}}}^* \ge x_{k=P_{\text{des}}}^* \tag{C10}$$

We denote the NLP model described by Eqs. C6–C10 as M1. To determine the values of the parameters μ_m and $\theta_{k,m}$ for which M1 is a reasonable approximation of the NAPDE model, we use the following parameter estimation model with cross validation.

Parameter estimation model

First, the following sets are defined:

SMB $\in S$: set of samples to be used for exact interpolation

SCV $\in S$: set of samples to be used for cross validation

The objective of the parameter estimation model is to minimize the prediction errors using a Euclidean distance metric as follows

$$\text{MIN} \sum_{i\in \text{SCV}} \left(\frac{\hat{y}_{i,m}-y_{i,m}}{y_{i,m}}\right)^2 \tag{C11}$$

subject to

$$\hat{y}_{i,m}=\mu_m+\sum_{j\in \text{SMB}} c_{j,m}u_{i,j,m} \quad i \in \text{SCV}, m \in M \tag{C12}$$

$$y_{i,m}=\mu_m+\sum_{j\in\mathrm{SMB}} c_{j,m}u_{i,j,m} \quad i\in \mathrm{SMB}, m\in M \tag{C13}$$

$$c_{i,m}=\sum_{j\in\mathrm{SMB}} v_{i,j,m}\left(y_{j,m}-\mu_m\right) \quad i\in \mathrm{SMB}, m\in M \tag{C14}$$

$$\sum_{i'\in\mathrm{SMB}} u_{i,i',m}v_{i',j,m}=I_{i,j,m} \quad i\in \mathrm{SMB}, j\le i, m\in M \tag{C15}$$

$$u_{i,j,m}=\exp\left[-\sum_k \theta_{k,m}\left(x_{i,k}-x_{j,k}\right)^2\right] \quad i\in S, j\in \mathrm{SMB}, m\in M \tag{C16}$$

Manuscript received Dec. 23, 2013, and revision received Feb. 23, 2014.